早稲田大学審査学位論文

博士（人間科学）

Molecular mechanisms regulating brain development
脳構築機構を制御する分子メカニズムの解明

2022 年 1 月

早稲田大学大学院　人間科学研究科

山田　晴也

YAMADA, Seiya

研究指導担当教員：　榊原　伸一　教授

Contents

Introduction

Mammalian cortical development

The spatiotemporal differentiation of neural stem/progenitor cells (NSPCs) into immature neurons and neuronal migration are necessary for the proper development of the central nervous system (CNS). The cerebral cortex of embryonic mice contains two distinct types of NSPCs: paired box 6-positive ($Pax6^+$) apical progenitor cells (radial glia), located in the ventricular zone (VZ), and T-box brain protein 2-positive ($Tbr2^+$) basal progenitor cells (intermediate progenitor cells), which are located the in subventricular zone (SVZ) (Englund et al., 2005). In the neocortex, newborn neurons generated from NSPCs migrate radially toward the cortical plate, accompanied by sequential changes in cell shape. Neurite outgrowth and ensuing polarity formation in immature neurons are also required for cortical layer stratification, and defects in neuronal migration not only cause brain malformation but also various psychiatric disorders, including epilepsy and mental retardation (Hansen et al., 2017; Represa, 2019).

Purinosome

Purines, compounds containing a pyrimidine ring fused with an imidazole ring, are found in all living species, and include the nucleobases adenine and guanine (Traut, 1994). Apart from their critical function as the building blocks of DNA (deoxyadenosine and deoxyguanosine) and RNA (adenosine and guanosine), purines work as components of essential biomolecules and as a source of second messenger molecules (cyclic AMP and cyclic GMP), cofactors coenzyme A and nicotinamide adenine dinucleotide (NADH), cellular energy substrate ATP, and GTP which is

essential for the signal transduction of many G-proteins. Other purine derivatives contain hypoxanthine, xanthine, and uric acid. Specifically, purines function as neurotransmitters in the brain by acting upon purinergic receptors. Purine metabolites, including ATP and GTP/GDP, are crucial for polarity formation in postmitotic cortical neurons (Raman et al., 2018). During brain development, purinergic signaling is essential for NSPC maintenance and neuronal migration in the neocortical SVZ (Lin et al., 2007; Liu et al., 2008).

In mammalian cells, purine content is regulated by a coordinated balance between the *de novo* and salvage biosynthetic pathways. Although the cellular purine pool is usually supplied by the recycling of degraded bases *via* the salvage pathway, the d*e novo* pathway is upregulated under cellular conditions demanding higher levels of purines, such as tumor growth and cell expansion (Yamaoka et al., 1997). *De novo* purine synthesis comprises a series of 10 enzymatic reactions and is mediated by six evolutionarily conserved enzymes [phosphoribosyl pyrophosphate amidotransferase (PPAT), phosphoribosylglycinamide formyltransferase (GART), formylglycin-amidine ribonucleotide synthase (FGAMS), phosphoribosylaminoimidazole carboxylase phosphoribosylaminoimidazole succinocarboxamide synthetase (PAICS), adenylosuccinate lyase (ADSL), and 5-aminoimidazole-4-carboxamide ribonucleotide formyltransferase inosine monophosphate (IMP) cyclohydrolase (ATIC)], to produce IMP from phosphoribosylpyrophosphate (Baresova et al., 2018). The enzymes that catalyze *de novo* purine synthesis are assembled near mitochondria and microtubules as a huge multienzyme complex called “purinosome” (An et al., 2010; An et al., 2008; French et al., 2016). Purinosome is a dynamic and functional giant protein complex that emerges during high levels of cellular purine demand in mammalian cultured cells (An

et al., 2008). Purinosome formation is linked to cell division (Chan et al., 2015). Furthermore, the dynamic assembly and disassembly of purinosomes *in vivo* might be crucial for the proper development of the human brain. Mutations in *ADSL* and *ATIC* genes cause severe developmental brain defects, such as mental retardation, autistic features, epilepsy, microcephaly, and congenital blindness (Jurecka et al., 2015; Marie et al., 2004). The bifunctional enzyme PAICS, another component of the purinosome, is associated with prostate and breast cancer metastasis and proliferation (Barfeld et al., 2015; Chakravarthi et al., 2018; Meng et al., 2018). PAICS deficiency in humans was recently reported. A missense mutation in *Paics* causes the severe phenotype with multiple malformations, including a small body, short neck, and craniofacial dysmorphism, resulting in early neonatal death (Pelet et al., 2019). To date, however, there is no direct evidence of the localization or physiological function of purinosomes during brain development.

In this study, we identified Nwd1 (NACHT and WD repeat domain-containing protein 1) as a novel signal transduction ATPases with numerous domains (STAND) family member expressed in NSPCs. In addition, we revealed Nwd1 regulates NSPC proliferation and neuronal migration through the control of purinosome formation during cortical development.

Materials and Methods

Animals

ICR male mice were purchased from Japan SLC Inc. (Shizuoka, Japan). The date of conception was established by the presence of a vaginal plug and recorded as embryonic day zero (E0). The day of birth was designated as P0. Mice were housed

under temperature- and humidity-controlled conditions on a 12/12 h light/dark cycle, with *ad libitum* access to food and water. All protocols were approved by the Committee on the Ethics of Animal Experiments of Waseda University.

Tissue preparation

Pups and 10-week-old adult male mice were anesthetized with an intraperitoneal injection of sodium pentobarbital (10 mg/kg) and perfused transcardially with saline solution, followed by 4% paraformaldehyde (PFA) in 0.1 M phosphate buffer (pH 7.4). Brains were dis- sected and postfixed in the same fixative overnight at 4°C. Embryos at E13.5, E16.5, and at E18.5 were perfused through the cardiac ventricle with 4% PFA, followed by postfixation overnight at 4°C. Embryos at E10.5 were fixed by immersion into the fixative for 4 hr. Fixed embryos and postnatal or adult brains were cryoprotected in 30% sucrose in phosphate buffered saline (PBS) overnight at 4°C and embedded in optimal cutting temperature compound (Sakura Finetek, Tokyo, Japan). Frozen sections of embryos and postnatal brains were cut at a thickness of 14 μm, using a cryostat and collected on MAS coated glass slides (Matsunami Glass, Osaka, Japan). For adult brains, free-floating sections were cut at 30 μm and stored at −20°C in antifreeze liquid (30% glycerol, 30% ethylene glycol in PBS).

Plasmid vectors

Mouse *Nwd1* cDNAs were subcloned into the pEGFP-C2 vector (Clontech Takara Bio) to express the Nwd1 protein fused with EGFP. The *Nwd1* and *EGFP-Nwd1* cDNAs were subcloned into the pCAGGS vector (a gift from Dr. Jun-ichi Miyazaki, Osaka University, Japan). For the yeast two-hybrid (Y2H) screening, *Nwd1* cDNAs corresponding to the N-terminal portion of the protein (accession number BC082552; 4bp–1026bp) were subcloned into pGBKT7 (Clontech Takara Bio) to express the N-

terminal domain of Nwd1 fused with the GAL4 DNA-binding domain. The Flag-tagged human NWD1 expression plasmid was provided by Dr. Correa (Sanford-Burnham Medical Research Institute, Canada) (Correa et al., 2014). *pFGAMS-EGFP* and *pPAICS-EGFP* (#99108) were gifts from Dr. Stephen Benkovic (Addgene plasmids # 99107 and # 99108, respectively) (An et al., 2008). HSP90-HA was a gift from Dr. William Sessa (Addgene plasmid #22487) (Cardena et al., 1998). *pCAG-DsRED* was a gift from Dr. Connie Cepko (Addgene plasmid # 11151) (Matsuda and Cepko, 2004).

shRNA expression vectors

We purchased a MISSION shRNA vector library encoding the microRNA-adapted shRNA targeting mouse *Nwd1* (Sigma-Aldrich). Among five shRNA clones (TRCN0000257630, TRCN0000247062, TRCN0000257635, TRCN0000257616, and TRCN0000179877), TRCN0000247062 and TRCN0000257635 yielded efficient knockdown of the exogenous Nwd1 and EGFP-Nwd1 expressed in cultured cells; these clones were designated as shRNA #1 and shRNA #2, respectively (Figure 5A–5E) The targeting sequences of shRNA #1 and shRNA #2 were: 5′–TACGACTGTGCATGCTCTAAA–3′ and 5′–CAGGTAATCCAAGTTCGATAT–3′, respectively. The two constructs targeted the coding region of the Nwd1 mRNA. We also used MISSION shRNA plasmids for mouse *Paics* (Sigma-Aldrich). Among five clones (TRCN0000076100, TRCN0000076101, TRCN0000076102, TRCN0000076098, and TRCN0000076099), TRCN0000076101, TRCN0000076102, and TRCN0000076098 were designated as shRNA #1, shRNA #2, and shRNA #3, respectively (Figure 5F). The targeting sequences for shRNA #1, shRNA #2, and shRNA #3 were 5′–CTGCTCAGATATTTGGGTTAA–3′, 5′–GCTGATGTCATTGATAATGAT–3′, and 5′–GCACCTGCTTTCAAATACTAT–3′,

respectively. shRNA #1 and shRNA #2 targeted the coding region, whereas shRNA #3 targeted the 3′ untranslated region (3′-UTR) of the *Paics* mRNA. A non-targeting shRNA (# SHC202) was also purchased from Sigma-Aldrich.

Production and purification of anti-Nwd1 antibodies

The polyclonal antibody for Nwd1 was raised in rabbits by immunizing them with a KLH-conjugated peptide (Biologica Co, Nagoya, Japan), corresponding to amino acids 706–725 of the mouse Nwd1 protein (N-LITLPLVGKPLNLDRKVAPQ-C) (GenBank accession no. XM_006531086). This antigenic peptide sequence corresponds to the middle region of the protein, adjacent to the cluster of WD40 repeats. It is conserved across species, including mouse, rat, wolf, cattle, chimpanzee, and human, and is the same sequence for the anti- genic peptide used to generate an Nwd1 antibody in a previous study (Correa et al., 2014). Antibodies were purified using the synthetic pep- tide coupled to sepharose resin, as previously described (Sakakibara et al., 2001). To confirm the specificity of the affinity purified antibody, antibodies were preabsorbed with the immunogenic peptides. Briefly, 50 μg of the synthetic peptides were incubated with 10 μg of the Nwd1 antibody at 4°C for 2 hr. The supernatant was tested by immunohistochemical and western blot analysis, as described below.

Primary antibodies

The following primary antibodies were used: anti-Nwd1 (affinity-purified rabbit polyclonal antibody, 1:200 for immunostaining, 1:2000 for immunoblotting), anti-Nwd1 (rabbit polyclonal antibody generated by immunizing the recombinant mouse Nwd1 protein; 1:500 for immunostaining, 1:5000 for immunoblotting), anti-Cytochrome C(mouse monoclonal clone 2D8D11, Proteintech, AB_2716798; 1:100 for immunostaining), anti-KDEL (mouse monoclonal cone 10C3, Stressgen Bioreagents,

AB_2314691; 1:400 for immunostaing), anti-CD31 (rat monoclonal clone ER-MP12, SRT Bio-Rad, AB_2161024; 1:100 for immunostaing), anti-Nestin (chicken polyclonal IgY, Aves Labs, NES; 1:4000 for immunostaining), anti-Nestin (rabbit polyclonal, IBL, 18741; 1:250), anti-α-tubulin (rabbit polyclonal, MBL, PM054; 1:2000 for immunoblotting), anti-GFP (chicken polyclonal IgY, Aves Labs, GFP-1010; 1:2000 for immunostaining), anti-GFP (rabbit polyclonal, GeneTex , GTX113617; 1:2000 for immunoblotting), anti-doublecortin (DCX) (goat polyclonal, Santa Cruz, sc-271390; 1:200 for immunostaining), anti-β-tubulin III (chicken polyclonal IgY, AVES Labs, TUJ; 1:1000 for immunostaining), anti-Pax6 (rabbit polyclonal, MBL, PD022; 1:1000 for immunostaining), anti-Tbr2 (chicken polyclonal, Merck Millipore, 633572; 1:1000 for immunostaining), anti-Ki67 (rabbit monoclonal clone SP6, Lab Vision, RM-9106; 1;1000 for immunostaining), anti-Paics (rabbit polyclonal, Proteintech, 12967-1-AP; 1:200 for immunostaining), anti-GFAP (mouse monoclonal clone G-A-5, Sigma-Aldrich, G3893; 1:400 for immunostaining), anti-SMI312 (mouse monoclonal, Biolegend, 837904; 1:1000, for immunostaining), anti-HA (rabbit polyclonal, MBL, 561; 1:200 for immunostaining, 1:2000 for immunoblotting), and anti-DDDDK (Flag) (mouse monoclonal, MBL, FLA-1; 1:10000 for immunostaining and immunoblotting).

Cell culture

HEK293T, HeLa, and Neuro2a (N2a) cells were cultured in Dulbecco's Modified Eagle Medium (DMEM) containing 10% fetal bovine serum (FBS), penicillin/streptomycin, and L-glutamine. In purine-depleted conditions, HeLa cells were cultured in RPMI 1640 medium supplemented with L-glutamine and 5% dialyzed FBS, as described previously (An et al., 2008; French et al., 2013).

NSPCs were isolated from the E12.5 telencephalon, seeded onto dishes coated with fibronectin and polyethylenimine (PEI) (Sigma-Aldrich), and cultured in Advanced DMEM/F-12 (1:1) (Life Technologies) supplemented with 15 μg/mL insulin (Life Technologies), 25 μg/mL transferrin (Life Technologies), 20 nM progesterone (Sigma-Aldrich), 30 nM sodium selenite (Sigma-Aldrich), 60 nM putrescine (Sigma-Aldrich), 20 ng/mL basic fibroblast growth factor (FGF2) (Merck Millipore), and 10 ng/mL epidermal growth factor (Merck Millipore). For the primary culture of cortical neurons, embryonic cerebral cortices at E16.5 were dissected and mechanically dissociated. After washing with Opti-MEM I (Life Technologies), cells were electroporated, seeded onto poly-D-lysine-coated dishes, and cultured in neurobasal medium containing 2% B27 (Life Technologies) and 1% GlutaMax (Life Technologies) for 1–3 days *in vitro* (div). For immunostaining, cultured cells were fixed with 4% PFA for 20 min at 4 ℃ and permeabilized in 0.05% Triton X-100 in PBS for 10 min.

Cell transfection

Cultured cell lines were transfected with plasmid DNA and PEI MAX (Polysciences) complexes (ratio of DNA to PEI MAX, 1:3, w/w) formed in Opti-MEM I by incubation for 15 min at room temperature. The DNA complexes were added to cell cultures together with Opti-MEM I for 3 h, followed by cultivation with serum containing complete DMEM. Mouse NSPCs were expanded *in vitro* as described above, and primary cortical neurons were electroporated using a NEPA21 Electroporator (Nepagene) according to the manufacturer's specifications (NSPCs: two pulses of 125 V for 5 ms with an interval of 50 ms; primary cortical neurons, two pulses of 275 V for 0.5 ms with an interval of 50 ms).

In utero electroporation

In utero electroporation experiments were performed as described previously (Yumoto et al., 2013). Briefly, pregnant mice were anesthetized via intraperitoneal injection of a mixture containing medetomidine, midazolam, and butorphanol, according to a previous protocol (Kawai et al., 2011). A DNA solution (5 μg/μL) in PBS with 0.01% Fast Green dye (Sigma-Aldrich) was injected into the lateral ventricle through the uterus wall, followed by electroporation. The following constructs were electroporated: *pCAG-Nwd1*, *pCAG-EGFP*, *pCAG-EGFP-Nwd1*, *pFgams-EGFP*, *Nwd1* shRNAs, *Paics* shRNAs, and non-targeting shRNA. Electric pulses were generated by NEPA21 (Nepagene) and applied to the cerebral wall using a platinum oval electrode (CUY650P5, Nepagene), with four pulses of 35 V for 50 ms with an interval of 950 ms. An anionic electrode was placed on the lateral cortex, to ensure the incorporation of DNA into the VZ/SVZ. Embryos were perfused at E16.5, E18.5, and P7 with 4% PFA through cardiac perfusion.

Western and northern blot analysis

Northern blot analysis of primary cultures was performed on the same membrane used in our previous study (Yumoto et al., 2013). For probe synthesis, cDNA fragments obtained by SSH, which correspond to nt 9,770–10,456 of mouse Nwd1 cDNA, were subcloned into the NotI/XhoI sites of the pcDNA3 vector (Life Technologies) and used to prepare digoxigenin (DIG)-labeled riboprobes. The hybridization, posthybridization washes, and immunodetection with the alkaline phosphatase (AP)-labeled anti-DIG antibody were performed according to the manufacturer's instructions (Roche Diagnostics, Risch-Rotkreuz, Switzerland). Hybridization signals were detected using CDP-Star (Roche Diagnostics) and visualized with a luminescent image analyzer (LAS-3000; Fuji Film, Tokyo, Japan). The integrity

and equal loading of the RNA was verified by re- probing with a glyceraldehyde-3-P dehydrogenase (Gapdh) probe.

For western blotting, tissue lysates were prepared by homogenization in RIPA buffer (25 mM Tris–HCl, pH 7.6; 150 mM NaCl; 1% NP40; 1% sodium deoxycholate; 0.1% SDS), containing protease inhibitors (cOmpleteTM, Mini Protease Inhibitor Cocktail; Roche Diagnostics, Tokyo, Japan), followed by centrifugation at 15,000 rpm for 10 min. Protein lysates were treated with sample buffer (62.5 mM Tris–HCl, pH 6.8; 3% SDS; 5% glycerol; 2% beta-mercaptoethanol), resolved on 8% SDS-PAGE gels, and electroblotted onto Immobilon-P membranes (Millipore, Billerica, MA) at 4 °C overnight, using a wet transfer apparatus in transfer buffer containing 25 mM Tris–HCl, 192 mM glycine, and 0.05% SDS. After blocking with 1% skim milk in TBST (150 mM NaCl, 10 mM Tris–HCl, pH 7.4, 0.1% Tween 20), membranes were incubated with the Nwd1 primary antibody, followed by incubation with the horseradish peroxidase (HRP)- conjugated anti-rabbit secondary antibody (1:20,000; GE Healthcare) for 1 hr. The chemiluminescent signal was detected using the Immobilon western chemiluminescent HRP substrate (Merck Millipore, Tokyo, Japan) and visualized using an LAS-3000 image analyzer (Fuji Film, Tokyo, Japan). Membranes were re-probed with α-tubulin anti- body (1:2,000; MBL, Tokyo, Japan).

In situ hybridization

In situ hybridization was performed as described previously (Iwasaki, Yumoto, & Sakakibara, 2015). Two different cDNA fragments of 969 bp and 678 bp corresponding to nt 1,320–2,289 and 2,826–3,504 of the mouse Nwd1 full-length cDNA (accession no. BC082552) were used to prepare the DIG-labeled antisense and sense riboprobes, respectively. Hybridization signals were detected with AP-conjugated

anti-DIG antibody, followed by incubation with 0.11 mM NBT (nitro blue tetrazolium) and 0.12 mM BCIP (5-bromo- 4-chloro-3-indoyl phosphate) in 6% polyvinylalcohol (PVA), 100 mM NaCl, 100 mM Tris–HCl pH 9.8, and 50 mM $MgCl_2$ at 37 °C. Both Nwd1 antisense probes showed an identical expression pattern, while the sense riboprobes exhibited no labeling above background.

Immunohistochemistry

For antigen retrieval, tissue sections were heated at 90–95 °C for 10 min in 10 mM sodium citrate buffer (pH 6.0), using a microwave, and then treated with 0.3% H_2O_2 in PBST (0.1% Triton X-100 in PBS) for 40 min at 25°C, to quench the endogenous peroxidase activity. Sections were blocked for 1 hr in 5% normal horse serum in PBST and incubated overnight at 4°C with primary antibodies, diluted in the same blocking solution. Sections were incubated with HRP-polymer linked anti-rabbit IgG reagent (ImmPRESSTM; Vector Lab, Burlingame, CA) for 2 hr, and the HRP signal was visualized using 0.25 mg/mL dia- minobenzidine and 0.03% H_2O_2. Each step was followed by four washes in PBST. Free-floating sections were mounted on glass slides, dehydrated, and coverslipped with Entellan New (Merck Millipore). For control sections, the primary antibody was omitted or replaced with normal rabbit serum.

For double immunostaining, frozen sections, which had been treated with antigen retrieval solution, were blocked for 2 hr, at 4°C, with 5% normal goat serum in PBST, and incubated overnight at 4°C in a cocktail of primary antibodies. After washing with PBST, sections were incubated with Alexa Fluor 488-, Alexa Fluor 555- (Life Tech- nologies), or DyLight 549- (Jackson ImmunoResearch, West Grove, PA) conjugated secondary antibodies [$F(ab')_2$ fragment]. After coun- terstaining with 2 nM

TOPRO3 or 0.7 nM Hoechst 33,342 (Life Technologies), sections were mounted and imaged using a confocal (FV3000, Olympus) or fluorescence inverted microscope (Axio Observer, Zeiss).

Immunoprecipitation

For immunoprecipitation, cells were washed in ice-cold PBS and lysed in ice-cold lysis buffer containing 50 mM Tris-HCl (pH 7.5), 150 mM NaCl, 2 mM EDTA, 1% NP-40, and protease inhibitors (cOmplete Mini Protease Inhibitor Cocktail, Roche Diagnostics) for 30 min at 4 ºC. Lysates were centrifuged at 15,000 rpm for 10 min and the supernatants were incubated with TrueBlot anti-rabbit or anti-mouse IP beads (Rockland) for 1 h (for preclearing). After centrifugation at 15,000 rpm for 10 min, the supernatants were incubated with the primary antibody for 1 h, followed by immunoprecipitation overnight at 4 ℃. Immunocomplexes were washed four times with 0.1% NP40 in PBS, followed by treatment with 2× sample buffer (125 mM Tris-HCl, pH 6.8, 4% SDS, 10% sucrose, and 0.01% bromophenol blue) and immunoblotting.

Yeast Two-hybrid Screening

To identify Nwd1-binding proteins in the CNS, a Y2H screening was performed using the Matchmaker Gold Yeast Two-Hybrid System (Clontech Takara Bio), according to the manufacturer's instructions. The sequence encoding the 340 N-terminal amino acid residues of mouse Nwd1 (BC082552; 4–1026 bp) was subcloned in frame into pGBKT7, to express the N-terminal region of Nwd1 (bait) fused with the GAL4 DNA-binding domain. As the prey, we used the normalized mouse brain library (Clontech Takara Bio, Normalized Mate & Plate Library, cat. # 630488), in which each clone was fused with the Gal4 DNA-activating domain (AD). Mated yeast clones were

selected using minimal synthetic defined (SD) medium with double dropout (Leu^- and Trp^-) supplement (Clontech Takara Bio) containing Aureobasidin A and X-α-Gal as the blue-colored colonies; this was followed by a second screening using the SD quadruple dropout (Leu^-, Trp^-, Ade^-, and His^-) selective medium (Clontech Takara Bio). After the elimination of duplicates containing the same AD/library plasmid via yeast-colony PCR, plasmids were rescued from yeast using the Easy Yeast Plasmid Isolation Kit (Clontech Takara Bio). Protein interactions were confirmed by co-transformation of the Nwd1 bait with each candidate prey plasmid into Y2H Gold yeast host cells, followed by sequencing of the cDNA inserts.

Statistical Analyses

All numerical data are expressed as means ± SEM. In two-group comparisons, Welch's *t*-test was used to assess the significance of the differences in cell distribution over the cortical layers, the number of neurites, or the number of purinosomes between different groups. In multiple-group comparisons, analysis of variance followed by Welch's *t*-test was used. The *p* values obtained were corrected for multiple testing using the Holm–Bonferroni correction. The number of axons was compared using the chi-squared test.

Results

Identification of *Nwd1*

To isolate genes regulating NSPCs, we used the suppression subtractive hybridization, by which we identified *Nwd1* (NACHT and WD repeat domain-containing protein 1) encoding for novel proteins in NSPCs. Nwd1 is highly conserved across species, including, mice, rats, cattle, monkeys, and humans. To confirm the

expression of Nwd1 mRNA, we probed a northern blot containing RNAs from mouse NSPCs, expanded in vitro, and from differentiated cells. As shown in Figure 1A, we detected a major transcript, at the expected size of 10 kb, highly expressed in the NSPC, but downregulated in the differentiated cell sample.

The open reading frame of MB61/Nwd1 mRNA encodes for a 1,573-amino acid protein with a predicted molecular mass of 175 kDa (XP_006531149; Figure 1B). Motif search analysis using BLAST and UniProt SMART algorithms (EMBL) showed that Nwd1 protein contained a NACHT domain in the central region (amino acids 337–504), followed by a cluster of 12 WD40 repeats at the C-terminus (Figure 1B). Based on recent sequence-based structure predictions, a large number of genes containing a P-loop NTPase signature NACHT [NAIP (neuronal apoptosis inhibitory protein), CIITA (MHC class II transcription activator), HET-E (incompatibility locus protein from Podospora anserina), and TEP1 (telomerase- associated protein 1)], domain have been classified as the clade of STANDs (Leipe et al., 2004). The STAND protein family often mediate ligand-induced self-oligomerization to form the giant multiprotein complex critical for various important cellular responses; e.g., the apoptotic peptidase activating factor 1 (Apaf1) and nucleotide-binding oligomerization domain-like receptors (NLRs) induce the assembly of large multiprotein complexes, the ‘‘apoptosome’’ and ‘‘inflammasome,’’ and play central roles in cell death and innate immune responses, respectively (Cai et al., 2017; Dorstyn et al., 2018; Leipe et al., 2004). By comparing the domain architecture, we found that Nwd1 was most similar to Apaf1, due to the presence of the clustered WD40 repeats, in the C-terminal region, as well as of the centrally located NACHT domain. However, the N-terminal region of Nwd1 lacked the CARD found in Apaf1, as well as the well-characterized effector

domains commonly found in numerous other STAND proteins. We hypothesized that this could infer the existence of an unidentified and unique effector domain in Nwd1. Indeed, using the InterPro database search (Finn et al., 2017), we found a short stretch of sequence, in the N-terminal region of Nwd1, which exhibited similarity to domain of unknown function 4,062 (DUF4062; IPR025139). DUF4062 signature is one of the phylogenetically conserved motifs, whose function remains unknown.

Tissue distribution of *Nwd1* mRNA in the embryonic and adult CNS

To examine the expression of Nwd1 in NSPCs in vivo, we performed in situ hybridization analysis using tissue from developing and postnatal brains. At E13.5, Nwd1 expression was observed in the VZ surrounding the ventricles where NSPCs were dividing (Figure 1C). In the postnatal brain, a strong signal was detected in the SVZ surrounding the lateral ventricles (Figure 1D) and in the rostral migratory stream (Figure 1E), where neuronal progenitors that are continuously generated in the SVZ migrate toward the olfactory bulbs to supply interneurons (Sakakibara & Okano, 1997; Zhao et al., 2008). In the adult rodent hippocampus, it is well documented that resident NSPCs in the sub- granular zone (SGZ), a thin layer between the granule cell layer and hilus of the hippocampal dentate gyrus, proliferate and give rise to new neurons that integrate into the existing circuitry of the dentate gyrus (Zhao et al., 2008). The NSPC population in the SGZ comprises slowly dividing radial glia-like cells and serves as the source of neurons during adult neurogenesis (Miller et al., 2013). As shown in Figure 1G, the strongest hybridization signal of Nwd1 mRNA was observed in the putative NSPCs aligning in the SGZ in the adult hippocampus. These results indicate the abundance of Nwd1 mRNA in NSPC populations throughout life. Nevertheless, Nwd1 mRNA was broadly detected in postmitotic neurons found outside the germinal zones,

albeit greatly lower levels, in the embryonic forebrain cortical plate and the olfactory bulb, most cortical and brain stem areas, as well as in the cerebellar Purkinje cell layer postnatally (Figure 1C–G).

Nwd1 expression in cultured NSPCs

To assess the distribution of Nwd1 using specific antibody in NSPCs, we immunostained cultured NSPCs that were isolated from E13.5 mouse cortices and maintained in a defined medium containing FGF2 and EGF. Cells in monolayer cultures of NSPCs frequently exhibit unipolar or bipolar morphology, resembling neuroepithelial cells in the embryonic VZ, and are thought to possess stem cell characteristics, namely, self-renewal and multipotent differentiation into neurons and glia (Yumoto et al., 2013). As shown in Figure 2, Nwd1 was intensely expressed in the cytoplasm and cellular processes of actively proliferating NSPCs. In addition, we found that Nwd1 co-localized with cytochrome c in NSPCs (Figure 2A–E). Cytochrome c is mainly localized at the outer mitochondrial membrane but is released from the mitochondria into the cytosol by various types of intracellular stress (Riedl & Salvesen, 2007). Apaf1 binds with and sequesters cytosolic cytochrome c to form the apoptosome, resulting in activation of the apoptotic pathway (Li et al., 1997). In the cellular processes of NSPCs, Nwd1 immunoreactivity coincided with cytochrome c-positive globular structures, which morphologically resembled mitochondria (Figure 2A–C, arrowheads). Partially overlapping expression of Nwd1 and cytochrome c was also found within the cell body (Figure 2D, E, arrowheads). In contrast, Nwd1 did not seem to be expressed in the ER. The anti-KDEL antibody is widely used to label the ER and ER- Golgi intermediate compartment (Pelham, 1990). As shown in Figure 2F, G, Nwd1

immunoreactivity did not overlap with KDEL-positive regions in NSPCs. These observations indicate that Nwd1 is found in cytosolic structures closely related with cytochrome c, outside the rough ER.

Nwd1 expression in the embryonic CNS

The E10.5 telencephalon is uniformly occupied by proliferating NSPCs (Sakakibara et al., 2001). Immunohistochemical analysis at this stage showed that Nwd1 was intensely expressed throughout the telencephalic wall (Figure 3A). These Nwd1-positive cells also expressed Nestin (Figure 3B), confirming the expression of the protein in stem cells. As neurogenesis progresses, mitotic NSPCs become restricted to the VZ lining the brain ventricles, while the newly born neurons occupy locations peripheral to the VZ (Sakakibara et al., 2001). At E13.5, the expression of Nwd1 was detected in the VZ of many CNS regions, including the telencephalon, ganglionic eminences, diencephalon, myelencephalon, and spinal cord, while robust expression was observed in postmitotic neurons migrating in the cortical plate of the forebrain (Figure 3C–E). Intense expression of Nwd1 in immature neurons was confirmed by co-labeling with the β-III tubulin antibody (Figure 3F). Thus, Nwd1 expression seems to be maintained in proliferating NSPCs and postmitotic neurons. Such an expression profile was consistent with our in situ hybridization data (Figure 1C). Outside the CNS, intense Nwd1 immunoreactivity was detected in peripheral neural crest-derived neurons, including sensory neurons of the trigeminal and dorsal root ganglia (Figure 3G), as well as in autonomic neurons of the sympathetic ganglia (Figure 3H).

Nwd1 expression in the developing cerebral cortex

Neurons and glial cells, originating from the embryonic VZ and SVZ, travel to appropriate layers to establish the stratified structure of the cerebral cortex; this process

lasts until the early postnatal period (Sakakibara et al., 2001). As shown in Figure 4, many Nwd1-positive cells were scattered throughout the gray matter of the neocortex from late embryonic stages into adulthood. Most of these cells morphologically appeared to be neurons, and Nwd1 immunoreactivity became more apparent in the cell body of terminally differentiated neurons. In contrast, the white matter, including the corpus callosum, contained few Nwd1-positive cells (Figure 4G). Between E16.5 and P0, lower but detectable Nwd1 immunoreactivity was observed in immature neurons migrating through the intermediate zone and accumulating in the cortical plate. Later, at P15, when terminal neuronal differentiation and synaptogenesis are almost completed (Sakakibara & Okano, 1997), elevated Nwd1immunoreactivity was detected in the cytoplasm of most neocortical neurons, including large pyramidal neurons within layers IV and V and medium-sized nonpyramidal neurons distributed throughout the cortex. In the adult cortex, a similar expression pattern was observed throughout the cerebral cortex regardless of the cortical area (somatosensory, motor, or entorhinal cortex) examined (Figure 4F). Furthermore, it should be noted that we also detected Nwd1 in blood vessels running through the brain parenchyma. Small aligned cells with elongated morphology, distinct from neurons, showed strong Nwd1 immunoreactivity in both embryonic and postnatal cortices (Figure 4C'). Co-immunostaining with CD31, a marker of endothelial cells, demonstrated that Nwd1 was found in CD31-positive endothelial cells of the capillary blood vessels at P7 (Figure 4H, I). In the adult brain, low Nwd1 immunoreactivity was observed in endothelial cells, suggesting that Nwd1 plays a role in growing blood vessels.

Nwd1 overexpression in vivo increases the NSPCs fraction and delays the radial migration of immature neuron

To investigate the role of Nwd1 in the developing cerebral cortex, we overexpressed the *Nwd1* gene *in vivo* using in utero electroporation. Full-length Nwd1 or control EGFP was electroporated into NSPCs in the developing dorsal neocortex at E14.5, a stage at which extensive neurogenesis and neuronal migration occurs. Electroporated embryos were harvested and analyzed after 48 h (at E16.5). To visualize the electroporated cells, the EGFP reporter plasmid was co-electroporated with the Nwd1 plasmid into the same embryos. Figures 5A–5C show that Nwd1 overexpression significantly suppressed neuronal migration from VZ, causing the accumulation of Nwd1-overexpressing cells in VZ/SVZ (control, 16.5 ± 4.2%, n = 6; Nwd1, 73.7 ± 6.0%, n = 6). At E16.5, the majority of cells electroporated with the control EGFP plasmid had migrated and reached the intermediate zone (IZ) and cortical plate (CP), where they became positive for Tbr1, a marker for post-mitotic neurons in the deep cortical layers and subplate (IZ, 72.3 ± 2.5%; CP, 11.2 ± 3.3%) (Figures 5A, 5T). However, Nwd1-overexpressing cells were rarely observed within the CP (Figures 5B, 5C, and 5U). Many $Nwd1^{+}$ cells remaining within the VZ/SVZ were positive for the neural stem cell marker Nestin (Figures 5D–5F) (control, 29.0 ± 6.0%, n = 4; EGFP-Nwd1, 73.8 ± 4.8%, n = 4), suggesting that they retained their NSPC nature and lined the ventricular wall for at least 2 days, without moving toward the pial surface. After 4 days (at E18.5), EGFP expression was observed in the $Brn2^{+}$ upper cortical layers (II–IV) and was almost absent in the $Brn2^{-}$ deep cortical layers (V and VI) or IZ in controls (Figures 5G and 5W). At this time, cells overexpressing Nwd1 remained in the lower layers of the neocortex, including IZ and SVZ (Figures 5H, 5I) (layers II–IV: control,

80.5 ± 1.2%, n = 4 versus Nwd1, 38.4 ± 6.1%, n = 4; layers V–VI: control, 8.3 ± 1.9% vs. Nwd1, 27.6 ± 2.7%; IZ: control, 11.3 ± 1.8% vs. Nwd1, 34.0 ± 5.7%). Within the $Brn2^-$ lower cortical layers, Nwd1-overexpressing cells exhibited the elongated bipolar morphology of traveling immature neurons (Figures 5H, 5X). These observations indicated that Nwd1 overexpression causes a significant increase in the $Nestin^+$ NSPC pool accumulating in the VZ/SVZ and delays the radial migration of immature neurons.

Nwd1 knockdown causes premature differentiation of NSPCs and represses neuronal migration

We explored the effect of Nwd1 loss of function on cortical development using small hairpin RNA (shRNA) delivery in vivo via in utero electroporation. Two different shRNA constructs (shRNA #1 and shRNA #2) targeting the coding region of mouse Nwd1 significantly reduced Nwd1 protein expression levels (Figure 5J). shRNA specificity was further demonstrated by Nwd1 immunostaining. Endogenous Nwd1 protein expression in cultured NSPCs was silenced by shRNA constructs (Figures 5K). We co-electroporated one of the shRNA constructs with an EGFP-expression plasmid into the neocortex at E14.5 and harvested embryos after 2 or 4 days. Then, we assessed the distribution of $EGFP^+$ cells among the discrete cortical zones. In control embryos, almost all $EGFP^+$ cells were found in either IZ or CP, and only a small fraction of cells was observed in VZ/SVZ at E16.5 (Figure 5L). However, Nwd1 knockdown (KD) resulted in a drastically reduced cell migration into the $Tbr1^+$ CP as a large number of cells remained in VZ/SVZ at E16.5 (% of cells in the VZ/SVZ: control, 15.7 ± 3.7%, n = 8; Nwd1 shRNA #1, 45.9 ± 4.2%, n = 4; Nwd1 shRNA #2, 42.2 ± 5.7%, n = 5) (Figures 5L–5O and 5V). We noticed that Nwd1 KD cells accumulated in IZ if they

were unable to penetrate the boundary between IZ and CP (Figures 5M and 5N). This phenotype was more pronounced after a further 2 days of shRNA expression. At E18.5, Nwd1 KD caused a significant accumulation of cells in IZ (control, 5.4 ± 2.0%, n = 4; Nwd1 shRNA #1, 56.8 ± 7.8%, n = 5) (Figures 5Y). Consequently, fewer Nwd1 KD cells reached the upper cortical layers (layers II–IV, control, 89.4 ± 1.3%, n = 4; Nwd1 shRNA #1, 32.0 ± 7.1%, n = 5; layers V–VI: control, 5.2 ± 1.0%; Nwd1 shRNA #1, 11.3 ± 1.4%). Many Nwd1 KD cells were still observed as $Brn2^{+}$ cells in the deep cortical layers (Figures 5P–5S and 5Y). These defects were rescued by overexpression of the human NWD1 homolog, which is resistant to targeting by the mouse Nwd1 shRNA. We co-electroporated Nwd1 shRNA and the full-length human NWD1 cDNA into the E14.5 cerebral cortex and performed analysis at E18.5. A large fraction of the electroporated cells reached the upper cortical layers through IZ (Figures 5Q and 5S) (% of cells in layers II–IV, 79.0 G 2.4%; layers V–VI, 14.8 ± 1.3%; IZ, 6.3 ± 1.6%, n = 10), restoring the cellular distribution comparable with that of the non-targeting control (see above). This finding further supported the notion that the loss of function of Nwd1 causes a severe migratory defect in immature neurons in vivo.

We reported the substantial expression levels of Nwd1 in the VZ/SVZ and immature neurons. Accordingly, a larger number of cells overexpressing Nwd1 remained within VZ/SVZ (Figure 5). Thus, we examined whether Nwd1 KD affected the nature of the NSPC pool in VZ/SVZ. At E18.5, i.e., 4 days after shRNA electroporation, double immunostaining revealed that the Nwd1 KD cells remaining in VZ/SVZ were positive for doublecortin (Dcx) (control, 13.6 ± 3.7%, n = 7; Nwd1, 68.7 ± 9.2%, n = 5) (Figures 6A–6F and 6S), which are markers of newborn immature neurons. Interestingly, Nwd1 KD drove many VZ cells to ectopically and prematurely

express Tbr2, a marker of the SVZ basal progenitor cells (intermediate progenitor cells) (control, 6.0 ± 3.9%, n = 4; Nwd1, 24.7 ± 4.7%, n = 4) (Figures 6G–6L' and 6T). Concurrently, we observed a decreased density of $Pax6^+$ apical progenitors in the VZ region, where Nwd1 shRNA was expressed (control, 47.2 ± 3.0%, n = 5; Nwd1, 25.6 ± 4.2%, n = 6) (Figures 6M–6S). Immunostaining for the mitotic marker Ki67 revealed that the proliferation rate of NSPCs was significantly reduced by Nwd1 KD (control, 27.1 ± 1.7%, n = 6; shRNA #1, 14.4 ± 2.3%, n = 6) (Figures 6U and 6V). To directly assess the effect of Nwd1 KD on NSPC proliferation, Nwd1 shRNA or control shRNA was transferred into primary cultured NSPCs then labeled with bromodeoxyuridine (BrdU). Following in vitro BrdU administration for 24 h, NSPCs were fixed after 0 or 24 h and the $BrdU^+$ cells were counted. Nwd1 KD significantly decreased the number of BrdU-incorporated NSPCs (labeling index at 0 h: approximately 45%; 24 h: approximately 35%) relative to the control (0 h: approximately 80%; 24 h: approximately 70%) (Figures 6W and 6X). Conversely, the silencing of Nwd1 in NSPCs resulted in an accelerated commitment to the neuronal lineage. A differentiation assay of NSPCs indicated that Nwd1 KD increased the fraction of b tubulin III^+ neurons (Figures 6Y and 6Z). Terminal deoxynucleotidyl transferase dUTP nick end labeling (TUNEL) staining of E16.5 brains revealed that Nwd1 KD did not induce apoptosis (control shRNA, 0.7 ± 0.3%, n = 8; Nwd1 shRNA, 1.2 ± 0.3%, n = 8) (Figures 7A–7E). Based on the early onset of lineage markers and decreased cell division rate in vivo and in vitro, we concluded that the loss of function of Nwd1 induced the cell-cycle exit and premature neuronal differentiation of NSPCs. Abnormally produced progenies might follow neuronal differentiation near their place

of birth, without proper cell migration, leading the apparent accumulation of $EGFP^+$ cells within the VZ/SVZ in addition to the IZ (Figures 5O and 6F).

Nwd1 knockdown causes periventricular nodular heterotopia

We examined postnatal brains after the embryonic KD of Nwd1. Embryos electroporated with control shRNA or Nwd1 shRNA at E14.5 were harvested at postnatal day 7 (P7), when neocortex stratification is almost complete. In a control experiment using a non-targeting shRNA, the electroporated cells were sparsely distributed in the entire cortical region, including the subcortical SVZ (Figure 8A). In contrast, Nwd1 KD pups frequently developed ‘‘periventricular heterotopia,’’ manifested by ectopic nodular masses in the lining of the ventricular wall (Figures 8B). These heterotopias were characterized by a lower cell density than the neighboring SVZ region and brighter nuclei, evidenced by Hoechst and hematoxylin staining (Figures 8A–8D). Most heterotopia-forming cells had large round cell bodies with few fine processes (Figures 8E and 8H), resembling neurons. Indeed, double immunostaining revealed that they were Dcx^+ neuron (Figures 8E–8J). Notably, these neurons expressed the vesicular glutamate transporter 1 (VGlutT1), and their somata were also closely surrounded by multiple $VGlutT1^+$ presynaptic terminals (Figures 8K–8P), implying the formation of excitatory circuits of glutamatergic neurons within a heterotopia. Conversely, these cells never exhibited labeling of the astrocyte marker GFAP (Figures 8Q–8V). Cellular architecture of this malformation was similar to the human periventricular nodular heterotopia composed of hyperexcitable neurons, which is a

developmental cortical dysgenesis frequently characterized by focal drug-resistant epilepsy (Battaglia et al., 2006).

Expression levels of Nwd1 is crucial for neurite outgrowth and axon formation of cortical neurons

To understand Nwd1 cellular function in postmitotic differentiating neurons, loss-of-function and gain-of- function experiments were performed using primary cultured cortical neurons. Nwd1 shRNA constructs were transferred into dissociated neurons prepared from E16.5 embryos and cultured for 3 days in vitro (div). In the control, a large fraction ($75%) of cells extended a single long axon immunostained for the SMI312 neurofilament marker (Figures 9A–9C). At this time, neurons transfected with Nwd1 shRNA #1 and shRNA #2 exhibited fewer SMI312^{+} axons (Figures 9D–9F), and a notable number of cells lacked axons (Figure 9G). We assessed whether Nwd1 overexpression affected axonal extension in each cortical neuron. Control cells electroporated with EGFP usually had a single axon after culture for 3 div (Figures 9H–9J). In contrast, EGFP-Nwd1 expression inhibited axonal extension (Figures 9K–9M). These cells occasionally had few short neurites that were devoid of SMI312 immunoreactivity. To visualize all immature neurites extending directly from soma, a plasmid encoding the red fluorescent protein dsRed was co-electroporated into the cortical neurons and the total number of neural processes was counted as neurites. We found that EGFP-Nwd1 overexpression reduced the number of neurites by almost half at 1, 2, and 3 div (Figures 9O–9U) (1 div: control, 4.0 ± 0.2; EGFP-Nwd1, 2.4 ± 0.2; 2 div: control, 4.6 ± 0.2; EGFP-Nwd1, 2.6 ± 0.2; 3 div: control, 5.3 ± 0.1; EGFP-Nwd1, 2.6 ± 0.2). Compared with the control, each neurite appeared thinner and unbranched,

suggesting early stage of neurite development. Consistently, in the embryonic cortex electroporated with Nwd1 shRNAs in utero, we observed a significant number of apolar cells within the IZ, which had round cell bodies, and it appeared as if they had failed to transform into migratory spindle-shaped neurons (arrows in Figure 7H and 7I). These results indicated that Nwd1 plays a vital role in axon formation in newborn neurons and that the highly controlled and just sufficient level of Nwd1 may be essential for axon and neurite outgrowth. Recent studies have indicated that dynamic changes in cell shape is closely coupled with the neuronal migration and cortical layer formation (Hirota and Nakajima, 2017). In the developing mammalian neocortex, newborn neurons transiently become multipolar cells with multiple neurites inside SVZ and lower IZ; thereafter, they undergo a change in morphology to a bipolar state before the onset of radial migration to the CP (Ohtaka-Maruyama and Okado, 2015); however, its molecular mechanism remains unclear. The defects in neuronal migration caused by manipulating Nwd1 might reflect a principal function of this gene in the morphological transformation of neurons during neurogenesis.

Nwd1 protein interacts with Paics

We attempted to understand the molecular mechanism by which Nwd1 regulates cortical development. We used a Y2H screen to identify proteins interacting with Nwd1. Based on its structural similarity to other STAND-family proteins (Leipe et al., 2004), we hypothesized that the N-terminal region of Nwd1 serves as an effector domain by which the protein binds signaling molecule(s) to trigger self-oligomerization mediated by the NACHT domain and WD40 repeats. The N-terminal region of Nwd1 contains a DUF4062 motif, a functionally uncharacterized motif found in bacteria and eukaryotes. The screening of a mouse brain library using a bait encoding the N-terminal

region of Nwd1 led to the isolation of 14 putative Nwd1-binding partners, including Abcd3, Clvs2, Ets1, Paics, Quaking, and Wdr74 (Table 1). Of these binding candidates, Paics was frequently isolated as independent cDNA clones. The interaction between Nwd1 and Paics in yeast was confirmed by the co-transformation of Nwd1 with the rescued Paics plasmid (Figures 10A and 10B). Paics is a bifunctional enzyme that catalyzes de novo purine synthesis and is composed of two distinct enzymatic domains: 4-(N-succinylcarboxamide)-5-aminoimidazole ribonucleo- tide synthetase (SAICARs, EC 6.3.2.6) activity in its N-terminal region and 5-aminoimidazole ribonucleotide carboxylase (AIRc, EC 4.1.1.21) activity in its C-terminal region. Since all Paics cDNAs identified by Y2H corresponded to the C-terminal region, encompassing AIRc activity domain (Table 1), it is likely that Nwd1 binds to Paics via this domain (Figure 10C). Nwd1–Paics interaction was further verified by a co-immunoprecipitation (co-IP) experiment using HEK293 cells expressing the FLAG-tagged full-length Nwd1 (FLAG-Nwd1) and EGFP-tagged full-length Paics (Paics-EGFP). Figure 10D shows that the Paics protein was specifically co-immunoprecipitated with FLAG-Nwd1.

Nwd1 and Paics are localized in purinosomes

We investigated the localization of Paics in the embryonic and postnatal mouse brain. An immunostaining analysis using an anti-Paics antibody showed high levels of Paics expression in the developing brain. At E10.5, Paics immunoreactivity was uniformly detected in the undifferentiated NSPCs in the telencephalon, extending from the VZ to the outer part of the neural tube (Figure 10E). We also noticed elevated Nwd1 expression in a small number of neurons that were b tubulin III^{+} and occupied the peripheral marginal zone (arrows in Figures 10E–10G). As CNS neurogenesis proceeds,

mitotic NSPCs become restricted to the VZ and the differentiated neurons form CP. Correspondingly, at E13.5, Paics expression was observed in many b tubulin III^{+} neurons in the CP, in addition to NSPCs lining the ventricular surface (Figures 10K–10M). At E18.5, a lower but detectable Paics expression level was observed in the cerebral cortex (unpublished data). This spatiotemporal expression pattern of Paics was highly comparable with that of Nwd1 (Figures 10H–10J and 10N–10P). Considering the equivalent distribution in the brain and its interaction with Paics, we hypothesized that Nwd1 is involved in the formation of the purinosome. To investigate the localization of Nwd1 in purinosomes, we examined the colocalization of Nwd1 with Paics or Fgams, both of which are used widely as purinosome markers. Because it is technically difficult to detect endogenously formed purinosomes, exogenously introduced markers (such as Fgams-EGFP) are generally used to label intracellular purinosomes (Pedley and Benkovic, 2017). Thus, HeLa cells that expressed FLAG-Nwd1 and Paics-EGFP or Fgams-EGFP transiently were cultured in purine-depleted media, to induce the formation of cellular purinosomes (An et al., 2008). Both the Fgams-EGFP and Paics-EGFP proteins exhibited a diffuse cytoplasmic distribution in purine-rich medium (Figures 11A–11C and 11G–11I). In the purine-depleted cells, however, many purinosomes became evident as the cytoplasmic clustering of Fgams-EGFP or Paics-EGFP (Figures 11D–11F and 11J–11L), as described previously (An et al., 2008). We observed the confined distribution and coclustering of FLAG-Nwd1 with Fgams-EGFP^{+} or Paics-EGFP^{+} purinosomes (arrows in Figures 11E and 11K). Such synchronously regulated coclustering of Nwd1 with Fgams and Paics during the purinosome formation allowed us to postulate that Nwd1 could also bind to Fgams. As

shown in Figure 11M, we performed a co-IP experiment using HEK293 cells and demonstrated the interaction of FLAG-Nwd1 with Fgams-EGFP.

A previous study that used co-IP with FGAMS followed by a proteomics analysis demonstrated that heat shock protein 90 (Hsp90) and Hsp70 colocalize in the purinosome (French et al., 2013). Knockdown of these chaperones leads to the disruption of purinosomes, implying the involvement of Hsp90/Hsp70 chaperone machinery in the protein complex assembly (French et al., 2013). The molecular chaperones Hsp70 and Hsp90 are ubiquitously expressed proteins that have many functions, including assisting in protein folding and stabilizing protein complexes (Makhnevych and Houry, 2012); however, their exact function in purinosome formation remains unclear (Pedley and Benkovic, 2017). To examine the colocalization of Nwd1 and Hsp90 in purinosomes, the distribution of EGFP-Nwd1 and HA-tagged Hsp90 (Hsp90-HA) was assessed in purine-depleted cells; we observed overlapping localization of Nwd1 in purinosomes (arrows in Figures 11N–11P). A co-IP assay of HEK293 cells expressing FLAG-Nwd1 and Hsp90-HA demonstrated an interaction between Nwd1 and Hsp90 (Figure 11Q). Consistent with this, Correa et al. showed that NWD1 binds to HSP90 in the human prostate cancer cell line, LNCaP (Correa et al., 2014). Taken together, these results strongly indicate that Nwd1 is a component of purinosomes. Conceivably, Nwd1 may act in cooperation with the chaperone machinery in purinosome assembly or stabilization.

Purinosome assembly is regulated by Nwd1 in NSPCs

To date, there is no evidence of the induction of purinosome assembly in nervous tissues. Therefore, next, we investigated whether NSPCs are capable of forming

purinosomes and whether Nwd1 localizes in these structures in NSPCs. NSPCs isolated from the E12.5 cerebral cortex and cultured as a monolayer frequently exhibit Nestin^{+} fine unipolar or bipolar processes, resulting in a morphology that resembles that of neuroepithelial cells in the embryonic VZ. The expression of Fgams-EGFP distinctly emerged as a granular structure (Figures 12A–12D). Immunostaining using the anti-Paics antibody indicated that a significant proportion of the endogenous Paics protein colocalizes in these clusters (Figures 12E, 12F). The colocalization of Fgams and Paics, which are two enzymes that are essential for de novo purine biosynthesis, strongly suggested that these clusters are functional purinosomes in the NSPCs. Purinosomes were often observed within the cellular processes, in addition to the cell body, under the plasma membrane of NSPCs (Figure 12F). Immunostaining with an anti-Nwd1 antibody revealed the localization of the endogenous Nwd1 protein in Fgams-EGFP^{+} purinosomes in NSPCs (Figures 12G–12L). The purinosome localization of Nwd1 became more evident after the introduction of EGFP-Nwd1 into NSPCs (Figure 12N). These data showed the presence of purinosomes in NSPCs.

To examine the role of Nwd1 in purinosome assembly, Nwd1 expression was suppressed by shRNA in NSPCs. Nwd1 shRNA constructs were electroporated into NSPCs expressing Fgams-EGFP. At 2 div, we counted the number of cells containing the functional purinosomes that are defined as the granules simultaneously labeled with Fgams-EGFP and endogenous Paics. As shown in Figure 12V, compared with the non-targeting shRNA (Figures 12P–12R), Nwd1 shRNAs reduced the number of cells containing Fgams- EGFP^{+} Pacis^{+} purinosomes considerably (Figures 12S–12U) (control, 58.3 ± 3.0%; shRNA #1, 35.0 ± 1.5%; shRNA #2, 34.7 ± 4.8%). Consistent with this, the fraction of cells that were labeled with Fgams-EGFP alone (Fgams-

EGFP^{+} Paics^{-}) was increased in NSPCs upon treatment with the shRNAs (arrowheads in Figure 12U). Because a protein complex lacking Paics no longer functions as a purinosome, we concluded that Nwd1 is required for the assembly of the functional purinosome in NSPCs.

Purinosome enzymes are essential for cortical development

To clarify the involvement of the purinosome in brain development, we examined the loss-of-function or gain-of-function phenotypes of Paics and Fgams. First, E14.5 embryos were electroporated in utero with Paics shRNAs to knockdown the expression of endogenous Paics (Figure 13D). As shown in Figure 13B, Paics shRNAs significantly repressed neuronal migration in the neocortex at least until 4 days post electroporation (E18.5). Compared with the non-targeting control shRNA, Paics KD resulted in a decreased number of neurons that reached the upper layers II–IV (control shRNA, 73.3 ± 4.8%, n = 8; Paics shRNA #1, 44.2 ± 8.2%, n = 4; Paics shRNA #3, 39.3 ± 5.8%, n = 9) (Figures 13A–13C). Instead, a considerable number of cells accumulated within the IZ and lower cortical layers (V–VI) of embryos expressing Paics shRNAs (IZ: control shRNA, 14.4 ± 3.3%, n = 8; Paics shRNA #1, 30.7 ± 7.3%, n = 4; Paics shRNA #3, 34.0 ± 6.1%, n = 9; layers V–VI: control shRNA, 12.3 ± 2.4%; Paics shRNA #1, 25.1 ± 1.2%; Paics shRNA #3, 26.8 ± 2.0%; Figure 13C). Notably, 4 days after Paics KD, a significant number of Paics KD cells persisted in the VZ/SVZ (Figure 13E). Immunostaining analysis revealed that these VZ/SVZ cells were Dcx, Tbr2 , and Pax6 (Dcx : control shRNA, 13.6 ± 3.7%, n = 7; Paics shRNA, 70.5 ± 4.4%, n = 4; Tbr2^{+}: control shRNA, 17.9 ± 2.4%, n = 4; Paics shRNA, 4.5 ± 2.1%, n = 4; Pax6^{+}: control shRNA, 47.2 ± 3.0%, n = 5; and Paics shRNA, 20.5 ± 10.0%, n = 4) (Figures 13E–13G and 13J). Consistently, most of these cells were negative for Ki67

(control shRNA, 29.6 ± 5.8%, n = 5; Paics shRNA, 7.5 ± 2.0%, n = 4) (Figures 13H–13J), indicating that Paics loss of function induced mitotic exit and premature differentiation of NSPCs. Next, we assessed the effect of Fgams overexpression on neurogenesis and neuronal migration in vivo. Fgams-EGFP was introduced into NSPCs in utero at E14.5. Fgams overexpression significantly suppressed neuronal migration from the VZ, leading to the accumulation of Fgams-overexpressing cells in the VZ/SVZ at E16.5 (control, 16.5 ± 4.2%, n = 6; Fgams, 80.3 ± 1.9%, n = 7) (Figures 13K–13M). Fgams-overexpressing cells were rarely observed within the IZ (control, 72.3 ± 2.5%; Fgams, 19.7 ± 1.9%). At E18.5, most Fgams- $EGFP^+$ cells remained in the IZ and SVZ (IZ: control, 11.3 ± 1.8%, n = 4; Fgams, 70.9 ± 5.9%, n = 8) and fewer cells were found in the cortical neuron layers (Figures 13N and 13P). The Fgams-$EGFP^+$ cells that accumulated in the germinal area were $Nestin^+$ (EGFP, 29.0 ± 6.0%, n = 12; Fgams-EGFP, 57.2 ± 6.5%, n = 4) (Figures 13Q–13R), suggesting that they were undifferentiated NSPCs. Taken together, these data provide strong evidence that both Paics and Fgams are essential for neurogenesis and corticogenesis and that the dysregulation of the genes that encode these proteins hinders neuronal migration. Such abnormal properties of neurons and NSPCs caused by the manipulation of Paics and Fgams seemed to be a phenocopy of Nwd1 overexpression/knockdown (Figures 5 and 6). It is likely that the de novo biosynthesis of purines, especially the tightly regulated levels of purinosome components, is indispensable for the orchestrated migration and differentiation of neurons that occur during brain development (Figure 14A).

Discussion

Nwd1 as a novel component of purinosomes

Here, we described the induction of the formation of Fgams^{+} Paics^{+} purinosomes in NSPCs. We also revealed that Nwd1 interacts with Paics and is localized in purinosomes in NSPCs. Nwd1 functions as a component in the assembly of purinosomes. Nevertheless, Nwd1 has no enzymatic activity related to purine biosynthesis, unlike Paics and Fgams. It is possible that Nwd1 participates in the assembly of purinosomes as a member of the STAND family of proteins. The STAND proteins are a newly recognized ATPases associated with diverse cellular activities (AAA) type of ATPases that act as signaling hubs and mediate the energy-dependent remodeling of proteins and the translocation of macromolecules. Generally, STAND genes encode multidomain proteins, typically encompassing an N-terminal effector domain, a centrally located NACHT domain that has P loop ATPase activity and mediates self-oligomerization, and a C-terminal ligand-binding domain (Leipe et al., 2004). The binding of specific ligands onto the C-terminal domain elicits a conformational change in STAND proteins, which is dependent on ATP levels; this results in the formation of the oligomeric ring-shaped superstructures of STAND proteins, which exhibit a central pore (Mermigka et al., 2020). Such superstructures serve as the tightly regulated molecular switch that controls diverse biological processes, including apoptosis and innate immune responses, in which the ring-like superstructures of STAND proteins drive the translocation or remodeling of the substrate proteins (Mermigka et al., 2020).

Among the STAND-family proteins, Nwd1 shares a similar domain structure with Apaf1 (Dorstyn et al., 2018; Leipe et al., 2004). During apoptosis, the C-terminal WD40 domain of Apaf1 binds to the cytochrome c molecules that leaked from damaged mitochondria. This ligand binding induces the energy-dependent self-oligomerization of

Apaf1. Subsequently, the ring-like superstructure of Apaf1 tethers caspase 9 through the N-terminal CARD domain of Apaf1 to form the macromolecular complex named apoptosome, which triggers the apoptotic caspase cascade (Zou et al., 1999). Similarly, Paics is assembled as a homo-octameric structure in purinosomes (Li et al., 2007), similar to the caspase 9 heptamer in apoptosomes. Based on these observations, we postulated that Nwd1 undergoes an ATP- dependent conformational change upon binding to the ligand(s), via which Paics proteins are triggered to be recruited to a purinosome (Figure 14B). Primary complex of Nwd1/Paics and several chaperones including Hsp90 might systematically tether other core enzymes, including Fgams, Ppat, and Gart to form an integrated purinosome (Figure 14B). This complicated molecular machinery may explain why the in vitro reconstitution of a functional purinosome has been unsuccessful thus far. Nwd1 may act as a sensor protein that drives the assembly and disassembly of purinosomes and activates the de novo purine biosynthesis pathway during CNS development.

Purinosome components regulate the maintenance of NSPCs and neuronal migration during cortical development

The present study,we reported the strong expression of Nwd1 in NSPCs and immature neurons during the development of the rodent brain. We also revealed a similar distribution of Paics and Nwd1 in the developing neocortex. The gain and loss of function of Nwd1, Paics, and Fgams, which were achieved using in utero electroporation, demonstrated that these purinosome components are essential for proper cortical development and that their dysregulation leads to a severe delay in the migration of immature neurons (Figure 14A). In addition, in vivo knockdown of Nwd1

resulted in a decrease in the number of $Pax6^{+}$ apical progenitors, in conjunction with the ectopic emergence of $Tbr2^{+}$ basal progenitor cells in the embryonic VZ. A previous study reported that the forced expression of the Tbr2 transcription factor directs the conversion of radial glia into basal progenitor cells (Sessa et al., 2008). Thus, we assumed that the altered expression level of Nwd1 caused the premature differentiation of NSPCs, suggesting a vital role for this protein in the maintenance of NSPC pools, including CNS stem cells (Figure 14A). Consistently, a previous study suggested a possible role for Nwd1 in tumor cells endowed with stem-cell-like properties, i.e., the proliferative and self-renewing properties. The expression of Nwd1is strikingly upregulated by Sox9, a transcription factor in malignant prostate tumor cells (Correa et al., 2014). A gain- and loss-of-function study indicated that Sox9 plays a central role in the specification and maintenance of CNS stem cells that reside in the embryonic VZ and adult SVZ (Scott et al., 2010). As a downstream target of Sox9, Nwd1 may have a function in the maintenance of CNS stem cells. Interestingly, it was also demonstrated that Paics is necessary for the proliferation and invasion of prostate cancer cells and that the silencing of Paics expression abrogates the progression of several types of prostate tumors (Chakravarthi et al., 2018). Taken together with this evidence, our findings imply that the formation of the purinosome machinery is crucial for the maintenance of somatic stem cells and tumor cells, which commonly require a large amount of de novo purine production.

In addition, we demonstrated that a tight control of the level of expression of Nwd1 is crucial for neurite extension and axon formation and that altered levels of expression of the Nwd1 gene caused migration defects in cortical neurons in vivo. Considering that the spatiotemporally controlled outgrowth of neurites is needed for the

establishment of neuronal polarity and neuronal migration (Hansen et al., 2017), purinosome formation might be closely linked to the dynamic morphological transformation of migrating neurons that occurs during corticogenesis. Purines affect many aspects of neuronal differentiation. For example, the activation of Rac, which is a small GTP-binding protein, is required for the formation of the leading process in radially migrating neurons in the embryonic cerebral cortex (Konno et al., 2005). Nwd1 might affect discrete aspects of neural development, including neuronal migration and the maintenance of the NSPC pool, via the regulation of the assembly/disassembly of purinosomes.

However, de novo purine synthesis is energy intensive and required for numerous substrates; therefore, it has been thought that terminally differentiated neurons place greater reliance on the purine salvage pathway than the de novo pathway to achieve prompt repair of damaged DNA and prevent neurodegeneration. A previous in vitro quantitative analysis of purines using neuroblastoma cell lines demonstrated that the intracellular purine content increases as neuronal differentiation proceeds, whereas de novo purine synthesis decreases during neuronal differentiation (Gottle et al., 2013), suggesting that a regulated balance between the de novo and purine salvage pathway is critical for coordinated neuronal differentiation. However, the switching molecules that determine this balance remain unidentified. Our current study provides an insight into the machinery governing purine metabolism during nervous system development.

Implication of Nwd1 and purinosome components in neurological disorders

Downregulation of Nwd1 by shRNA expression in the embryonic cerebral cortex often caused the cortical dysgenesis similar to human periventricular nodular heterotopia (PH), a cortical malformation that is characterized by the formation of ectopic aggregates of neurons that line the lateral ventricle. These nod- ules exhibited a rosette-like structure and were filled with the glutamatergic neurons innervated by VgulT1^{+} excitatory terminals, indicating the formation of abnormal excitatory circuit. In humans, PH is associated with intractable epilepsy and intellectual disability (Cossu et al., 2018). Previous studies using a genetic animal model showed that PH is caused by the failure of the radial migration of newborn neurons from the VZ in addition to the abnormal proliferation of NSPCs (Li et al., 2015; Lian and Sheen, 2015); however, the molecular mechanisms underlying the development of PH are not fully understood. Thus, the disturbance of the purine de novo synthesis pathway may be associated, at least in part, with the mechanism underlying the pathogenesis of PH.

In addition to PH, purinosome-related genes are responsible for certain neurological disorders. Deficiency of ADSL in humans causes atrophy of distinct regions of the brain, including the cerebral cortex, in addition to hypomyelination and lissencephaly (Jurecka et al., 2015). Patients with ATIC mutation exhibit neurological symptoms, including profound mental retardation and epilepsy accompanied by various dysmorphic features (Marie et al., 2004). A previous study that used cultured fibroblasts from these patients demonstrated that ATIC and ADSL mutations destabilize the assembly of the purinosome to various degrees and that the ability to form purinosomes is correlated with the severity of the phenotype of individual patients (Baresova et al., 2012). Recently, PAICS deficiency was reported in humans. Patients carrying a ho-mozygous missense mutation in the PAICS gene exhibit multiple severe malformations,

including a small body and craniofacial dysmorphism, resulting in early neonatal death (Pelet et al., 2019). Although inactivating mutations in the human NWD1 gene have not been reported to date, it was recently shown that the neuronal expression of NWD1 is upregulated in patients with temporal lobe epilepsy (Yang et al., 2019). Using a mouse model of acute epileptic seizures, it was suggested that Nwd1 regulates the neuronal hyperexcitability of glutamatergic synaptic transmission in the adult brain (Yang et al., 2019). Therefore, Nwd1 might be involved in a mechanism of regulation of the synaptic transmission via the formation of purinosomes or other macromolecular complexes.

Figure and Legends

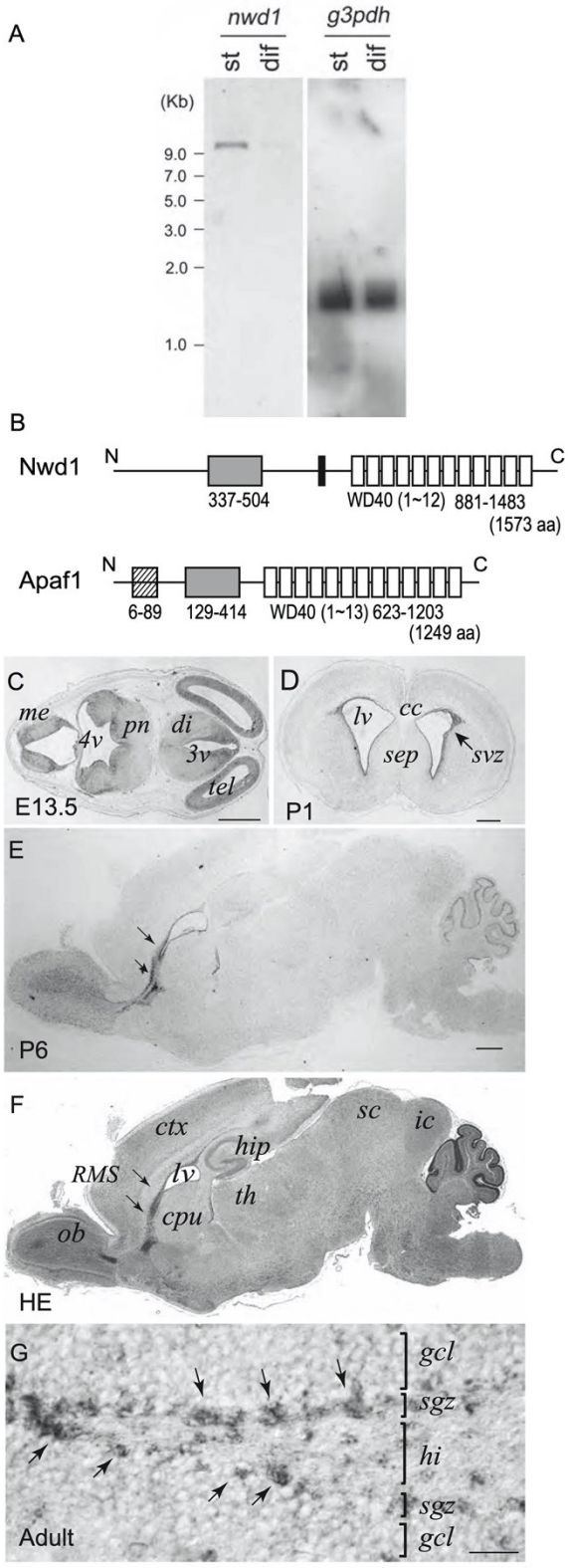

Figure 1. Identification of the mouse *Nwd1* gene

(A) Northern blot analysis showing the expression of Nwd1 mRNA in cultured embryonic NSPCs. st = NSPCs; dif = differentiated cells. Equal loading of RNAs was verified by re-probing the membrane with Gapdh (right panel). (B) Domain structure of the mouse Nwd1 and Apaf1 protein. Gray box, NACHT domain; open boxes, WD40 repeats; hatched box, CARD (caspase activation and recruitment domain). Solid bar indicates the peptide sequence used for the generation of the anti-Nwd1 antibody (706–725 aa). The accession numbers for Nwd1 and Apaf1 are XP_006531149 and NP_033814, respectively. (C–E) In situ hybridization showing the localization of Nwd1 mRNA in a transverse section of an E13.5 embryo (C), coronal brain section at P1, and sagittal section at P6. Arrows indicate the strong signals of Nwd1 mRNA in the SVZ (D) and RMS (E). (F) Hematoxylin–eosin-stained adjacent section to (E). (G) Dentate gyrus of adult hippocampus. Arrows in (G) indicate the SGZ cells that strongly express Nwd1 mRNA. tel = telencephalon; di = diencephalon; 3v = third ventricle; pn = pons; me = metencephalon; 4v = fourth ventricle; cc = corpus callosum; svz = subventricular zone; sep = septum; lv = lateral ventricle; ob = olfactory bulb; RMS = rostral migratory stream; ctx = cortex; cpu = caudate putamen; hip = hippocampus; th = thalamus; sc = superior colliculus; ic = inferior colliculus; sgz = subgranular zone; hi = hilus; gcl = granule cell layer of dentate gyrus. Scale bars represent 0.5 mm in C–F and 20 μm in G.

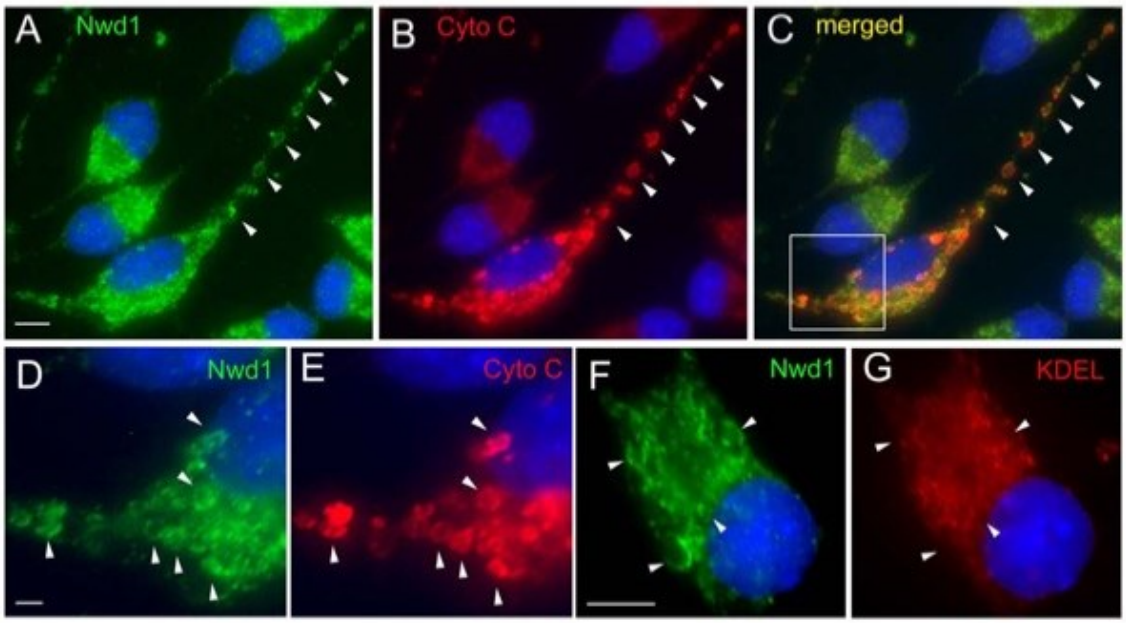

Figure 2. Nwd1 expression in cultured NSPCs

(A–C) Cultured NSPCs, expanding as a monolayer, were immunostained with the anti-Nwd1 (A, green) and anti-cytochrome c (B, red) antibodies. (D, E) Higher magnification of the boxed areas in A–C showing the co-localization of Nwd1 and cytochrome c. Nwd1 immunoreactivity is detected in cytochrome c-positive structures in the cell body and in the long fine NSPC processes (arrowheads). (F, G) NSPCs immunostained with the anti-Nwd1 (F) and anti-KDEL (G) antibodies. Nuclei are counterstained with Hoechst (blue). Note that most of Nwd1 immunoreactivity does not overlapped with the KDEL-positive rough endoplasmic reticulum (arrows). Scale bars represent 6 μm in A–C, 1 μm in D, and 5 μm in F.

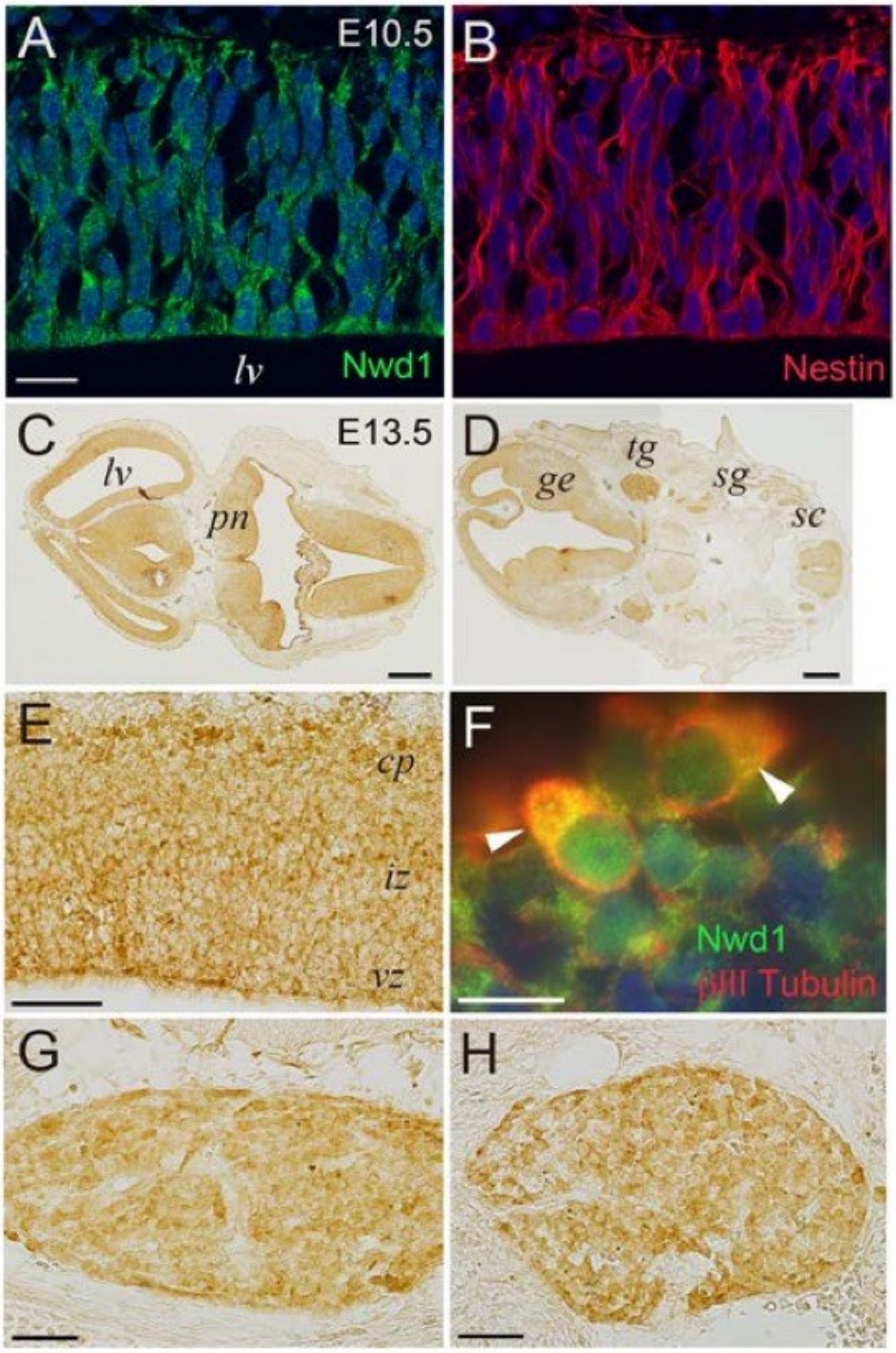

Figure 3. Nwd1 expression at embryonic stages

(A, B) Confocal images of E10.5 telencephalon stained with anti-Nwd1 (green) and anti-Nestin (red) antibodies. Nuclei are counterstained with TOPRO3 (blue). Note that Nwd1 is uniformly distributed in the neural tube neuroepithelium. (C, D) Transverse sections of an E13.5 head showing the immunolocalization of Nwd1 (brown). A section through the forebrain, midbrain, and pons is shown in C, while D depicts a section through the ganglionic eminence, medulla oblongata, and spinal cord. (E) Higher magnification of the area of the cerebral cortex surrounding the lateral ventricle in C. Nwd1 expression is found throughout the developing cortical layers. (F) The upper region of the cortical plate at E13.5 was double labeled with anti-Nwd1 (green) and anti-β-III tubulin (red) antibodies. Arrows demarcate immature neurons co-expressing Nwd1 and β-III tubulin. (G, H) Higher magnification images of the dorsal root (G) and sympathetic ganglia (H) at E13.5 showing Nwd1 expression in peripheral neurons. pn = pons; sg = sympathetic ganglia; ge = ganglionic eminence; sc = spinal cord; tg = trigeminal ganglion; lv = lateral ventricle; cp = cortical plate; iz = intermediate zone; vz = ventricular zone. Scale bars represent 15 μm in A and B, 370 μm in C and D, 50 μm in E, 10 μm in F, and 50 μm in G and H.

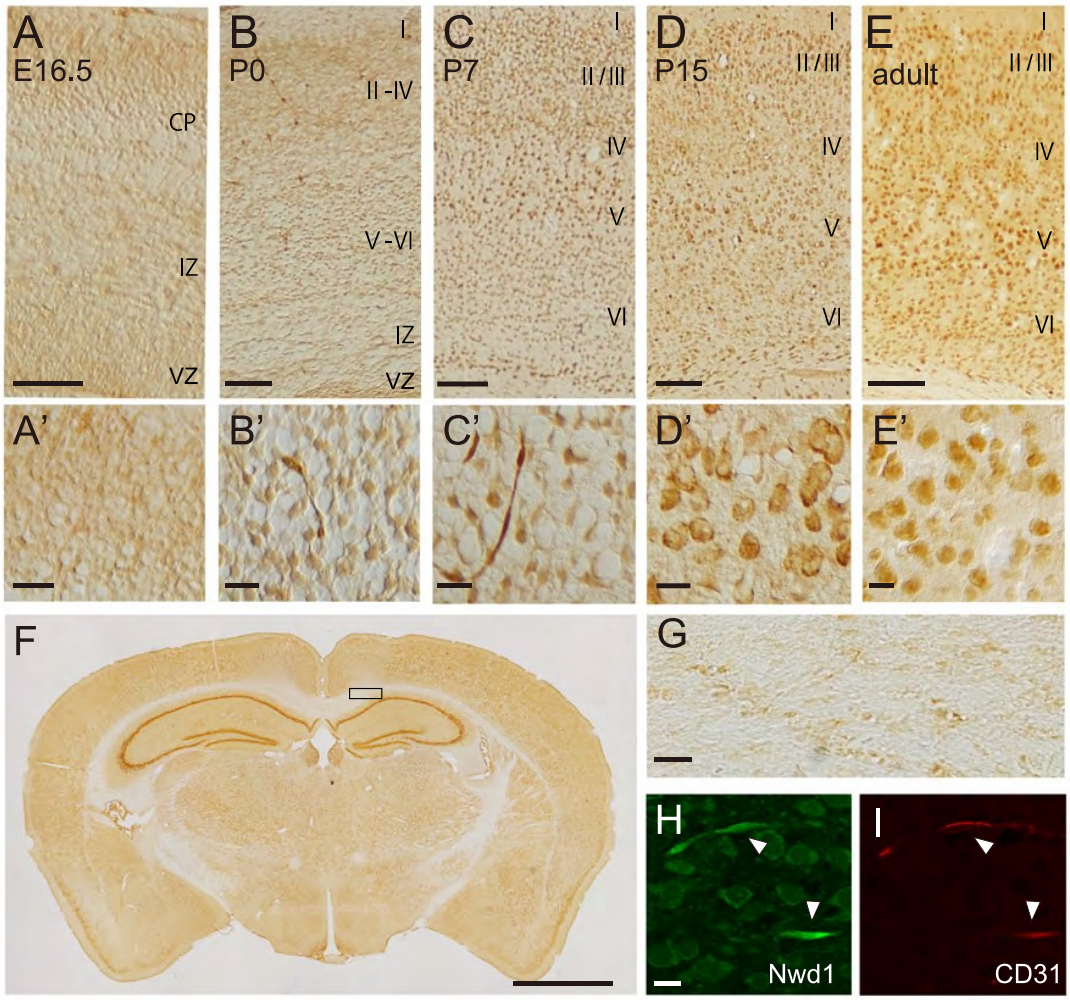

Figure 4. Nwd1 expression in the developing and adult cerebral cortex

Coronal sections of E16.5 (A, A'), P0 (B, B'), P7 (C, C'), P15 (D, D'), and adult (E, E') cerebral cortex showing the distribution of Nwd1-positive cells (brown). The pial surface is at the top. (A'–E') High-power photomicrographs of individual cells expressing Nwd1 in the gray matter, i.e., cortical plate or layers IV–V. Roman numerals represent the cortical layers. Nwd1 expression is mostly confined to neurons residing in the cortical gray matter at P15 and adult. Arrows indicate blood vessels. (F) Coronal section of an adult brain at the level of the anterior part of the hippocampus showing the ubiquitous distribution of Nwd1-positive neurons. Note the higher expression in

hippocampal pyramidal and granule neurons and entorhinal cortical neurons. (G) Enlarged view of the corpus callosum (rectangle area in F), showing the negligible levels of Nwd1 immunoreactivity in the white matter. (H, I) Co-immunostaining with anti-Nwd1 (H) and anti- CD31 antibodies (I), demonstrating Nwd1 expression in endothelial cells of capillary blood vessels at P7 (arrowheads). Scale bars represent 50 μm in A and B, 100 μm in C–E, 10 μm in A'–E', 1 mm in F, 10 μm in G, and 10 μm in H and I.

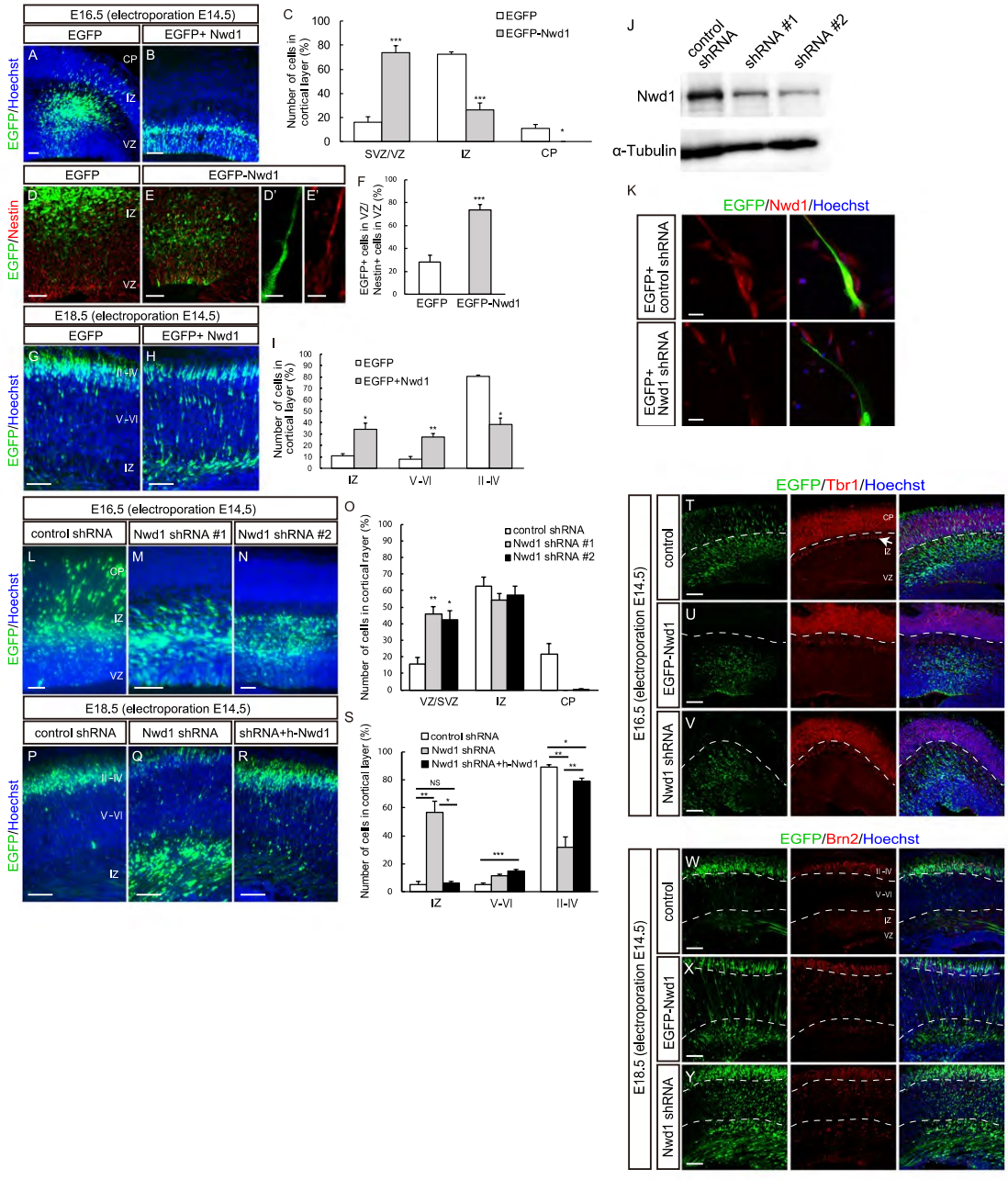

Figure 5. Dysregulation of Nwd1 disturbs the radial migration of neurons and directs NSPCs to reside in the VZ/SVZ

(A–I) Nwd1 overexpression in the embryonic neocortex. (A–C) In utero electroporation of control EGFP (A) or Nwd1 together with EGFP (B) was performed on E14.5, and the neocortex was analyzed at E16.5. (C) Distribution of electroporated

EGFP$^+$ cells in the indicated areas. *p < 0.05, ***p < 0.001, Welch's t test followed by Holm-Bonferroni correction. (D–F) EGFP-Nwd1 (E) or control EGFP (D) was electroporated at E14.5, and brains were immunostained for Nestin (red) at E16.5. (D' and E') Higher magnification of the VZ cells expressing EGFP-Nwd1 (D') and Nestin (E'). (F) Ratio of EGFP$^+$ or EGFP-Nwd1$^+$ cells to the total number of Nestin$^+$ cells in the VZ. ***p < 0.001, Welch's t test. (G–I) Nwd1 or control EGFP was electroporated at E14.5, and the brains were collected on E18.5. (I) Distribution of EGFP$^+$ cells in the indicated layers. *p < 0.05, **p < 0.01, Welch's t test followed by Holm-Bonferroni correction. (J) The non-targeting control or *Nwd1* shRNA (shRNA #1 or shRNA #2) was transfected into HEK293 cells that expressed EGFP-Nwd1 exogenously. The expression level of Nwd1 was evaluated by immunoblotting using an anti-Nwd1 antibody. Immunoblotting using an α-tubulin antibody was performed to ensure the equal loading of cell lysates. (K) The control shRNA or *Nwd1* shRNA #1 was transfected into the primary culture of NSPCs, together with EGFP. Cells were immunostained with an anti-Nwd1 antibody at 2 div, which showed that the expression of endogenous Nwd1 (red) was silenced by the *Nwd1* shRNA. (L–S) Nwd1 knockdown represses neuronal migration. An Nwd1 shRNA (shRNA #1 or shRNA #2) was co-electroporated with EGFP at E14.5 and cortices were analyzed at E16.5 (L–O) or E18.5 (P–S). (O) Distribution of EGFP$^+$ cells in the indicated areas at E16.5. *p < 0.05, **p < 0.01, Welch's t test followed by Holm- Bonferroni correction. (R) Nwd1 shRNA was co-electroporated with the full-length human NWD1 cDNA at E14.5, and the cortex was analyzed at E18.5. (S) Distribution of EGFP$^+$ cells in the indicated areas at E18.5. NS, not significant; *p < 0.05, **p < 0.01, ***p < 0.001, Welch's t test followed by Holm-Bonferroni correction. (T–Y) E14.5 embryos were electroporated *in utero* with

non-targeting control (T, W), EGFP-Nwd1 (U, X) or *Nwd1* shRNA #1 (V, Y) or, and brains were harvested at E16.5 (T–V) and E18.5 (W–Y). The shRNA constructs were co-electroporated with EGFP. (T–V) E16.5 brain sections were immunostained with anti-Tbr1 antibody (red), a marker for the deep cortical layer and subplate. Dashed lines represent the border between CP and subplate. Arrow in (T) indicates the $Tbr1^{+}$ subplate. (W–Y) E18.5 brain sections were immunostained with anti-Brn2 antibody (red), a marker for the upper cortical layers. Dashed lines denote the borders of upper layers (II–IV), deep cortical layers (V–VI) and IZ.

All data are presented as means G SEM. Scale bars, 50 μm in (A), (B), (D), and (L)–(N); 5 μm in (D') and (E'); 100 μm in (G), (H), (T)–(Y), and (P)–(R); 20μm in (K).

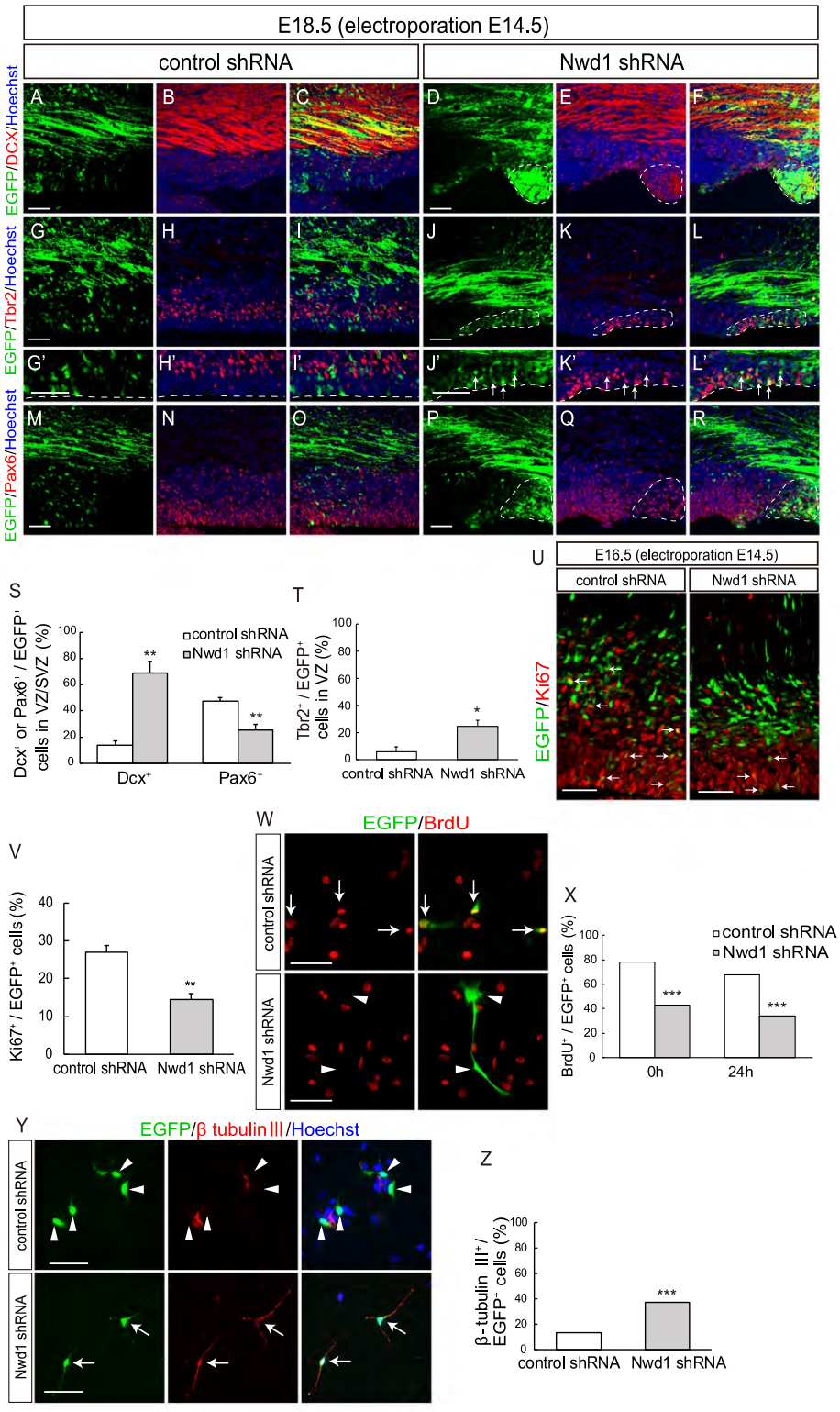
E18.5 (electroporation E14.5)
control shRNA
Nwd1 shRNA
EGFP/DCX/Hoechst
EGFP/Tbr2/Hoechst
EGFP/Pax6/Hoechst
A
B
C
D
E
F
G
H
I
J
K
L
G'
H'
I'
J'
K'
L'
M
N
O
P
Q
R
S
Dcx+ or Pax6+ / EGFP+ cells in VZ/SVZ (%)
control shRNA
Nwd1 shRNA
Dcx+
Pax6+
T
Tbr2+ / EGFP+ cells in VZ (%)
control shRNA
Nwd1 shRNA
U
E16.5 (electroporation E14.5)
control shRNA
Nwd1 shRNA
EGFP/Ki67
V
Ki67+ / EGFP+ cells (%)
control shRNA
Nwd1 shRNA
W
EGFP/BrdU
control shRNA
Nwd1 shRNA
X
BrdU+ / EGFP+ cells (%)
control shRNA
Nwd1 shRNA
0h
24h
Y
EGFP/β tubulin III/Hoechst
control shRNA
Nwd1 shRNA
Z
β-tubulin III+ / EGFP+ cells (%)
control shRNA
Nwd1 shRNA

Figure 6. Nwd1 knockdown causes the cell cycle exit and premature differentiation of NSPCs

(A–T) A control or Nwd1 shRNA was electroporated together with EGFP at E14.5, and the cortices were harvested at E18.5. Confocal images of sections stained with anti-Dcx (A–F), anti-Tbr2 (G–L’), and anti-Pax6 (M–R). (G’–L’) Higher magnification of the VZ cells shown in (G–L). The areas surrounded by dashed lines denote the distribution of cells that were electroporated with the Nwd1 shRNA (green), which remained in ZV/SVZ areas at E18.5. The VZ surface is outlined by the dashed line. (S) Quantification of $EGFP^+$ Dcx^+ or $EGFP^+$ $Pax6^+$ cells to total $EGFP^+$ cells in VZ/SVZ. Data are presented as means G SEM. **p < 0.01, Welch’s t test. (T) Quantification of $EGFP^+$ $Tbr2^+$ cells to total $EGFP^+$ cells in VZ. Data are presented as means G SEM. *p < 0.05, Welch’s t test. (U and V) An Nwd1 shRNA (U, right panel) or control shRNA (U, left panel) was co-electroporated with EGFP at E14.5, and the cortices were stained for the Ki67 mitotic marker (red) at E16.5. Arrows indicate $EGFP^+$ $Ki67^+$ cells. (V) Quantification of $EGFP^+$ $Ki67^+$ cells in relation to the total number of $EGFP^+$ cells. Data are presented as means G SEM. **p < 0.01, Welch’s t test.

(W and X) Primary cultured NSPCs were electroporated with control shRNA (W, upper panels) or Nwd1 shRNA (W, lower panels) together with EGFP, followed labeling with BrdU (red) for 24 h. Arrows indicate $EGFP^+$ $BrdU^+$ proliferating NSPCs. Arrowheads indicate $EGFP^+$ $BrdU^-$ cells. (X) Following BrdU administration, NSPCs were fixed at 0 or 24 h and the $BrdU^+$ cells were counted. The numbers of $EGFP^+$ $BrdU^+$ cells were compared using the chi-square test. ***p < 0.001, 0 h: control shRNA, n = 240; Nwd1 shRNA, n = 153; 24 h: control shRNA, n = 214; Nwd1 shRNA, n = 111.

(Y and Z) Primary cultured NSPCs, electroporated with control shRNA (Y, upper panels) or Nwd1 shRNA (Y, lower panels) along with EGFP, were treated for 24 h with differentiation induction medium containing 1% FBS, followed by immunostaining with b-tubulin III antibody (red). Nuclei were stained with Hoechst dye (blue). Arrows indicate $EGFP^+$ b-tubulin III^+ neurons. Arrowheads indicate $EGFP^+$ b-tubulin III^- cells. (Z) The numbers of $EGFP^+$ b-tubulin III^+ neurons were compared using the chi-square test. ***$p < 0.001$, control shRNA, n = 503; Nwd1 shRNA, n = 240.
Scale bars, 50 μm.

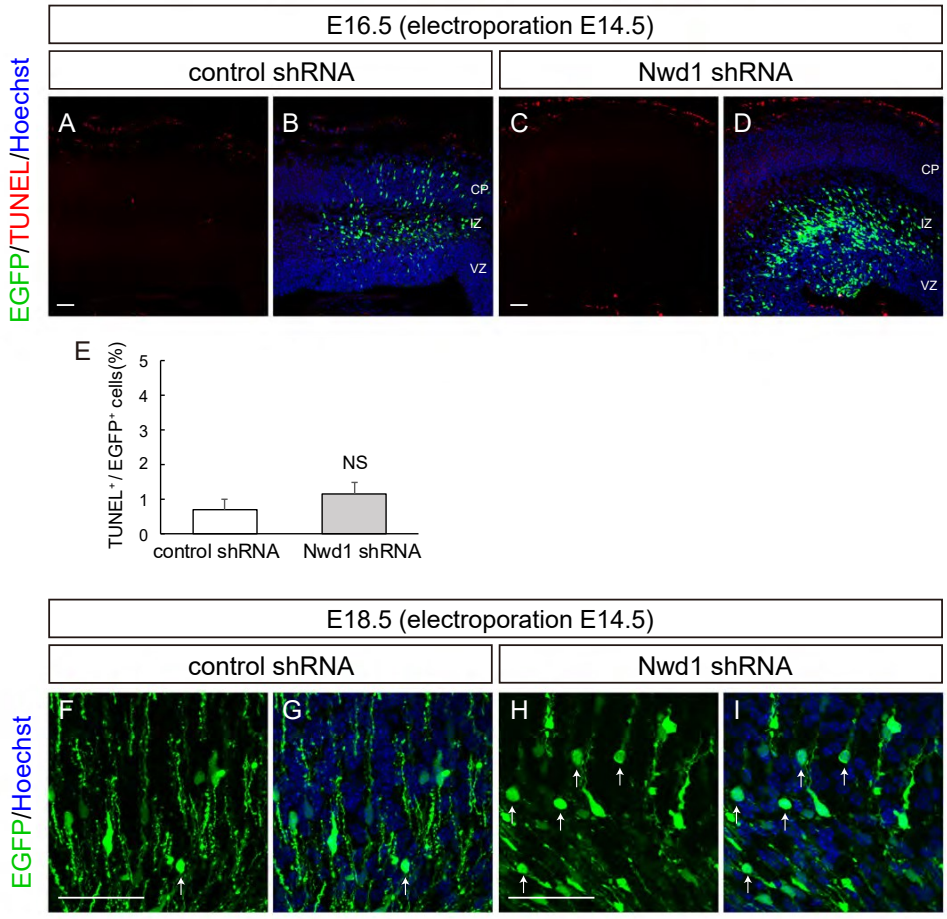

Figure 7. Nwd1 knockdown doesn't affect apoptosis

The non-targeting control or *Nwd1* shRNA #1 were electroporated into E14.5 brains along with EGFP, and embryos were harvested at E16.5 and E18.5. (A-E) Apoptotic cells were detected by TUNEL staining (red) at E16.5. (E) Number of $EGFP^+$ $TUNEL^+$ apoptotic cells. Control shRNA, n=8; Nwd1 shRNA, n=8. Data are presented as means ± SEM. NS, not significant, Welch's *t*- test. (F–I) Confocal projection images of E18.5 cerebral cortex. Note that the significant number of Nwd1 KD cells exhibited an apolar and round morphology (arrows) within the IZ. Nuclei are counterstained with Hoechst dye (blue). Scale bars, 50 μm.

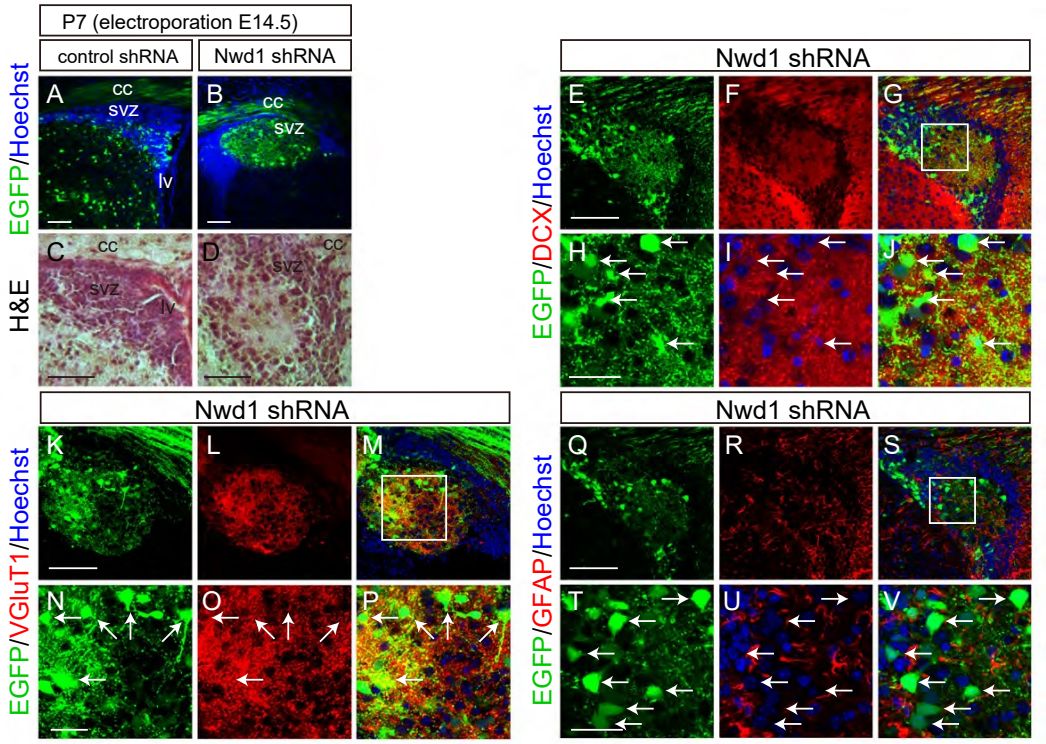

Figure 8. Nwd1 Knockdown Causes PH

(A–V) A control or Nwd1 shRNA was delivered into the brain together with EGFP on E14.5, and brains were collected on P7 (n = 5). (A and B) Sections through the SVZ area showing the development of periventricular heterotopia (HP) caused by Nwd1 KD (B). Nuclei are counterstained with Hoechst dye (blue). (C and D) Hematoxylin and eosin staining of HP. HP regions were immunostained using anti-Dcx (E–J), anti-VGluT1 (K–P), or anti-GFAP (Q–V) antibodies. (H–J), (N–P), and (T–V) are higher magnifications of the boxed areas shown in (G), (M), and (S), respectively. Arrows indicate the abnormally differentiated glutamatergic neurons that were Dcx, VGlut1 , and GFAP . cc, corpus callosum; lv, lateral ventricle. Scale bars, 100 μm in (A)–(G), (K)–(M), and (Q)–(S); 30 μm in (H)–(J), (N)–(P), and (T)–(V).

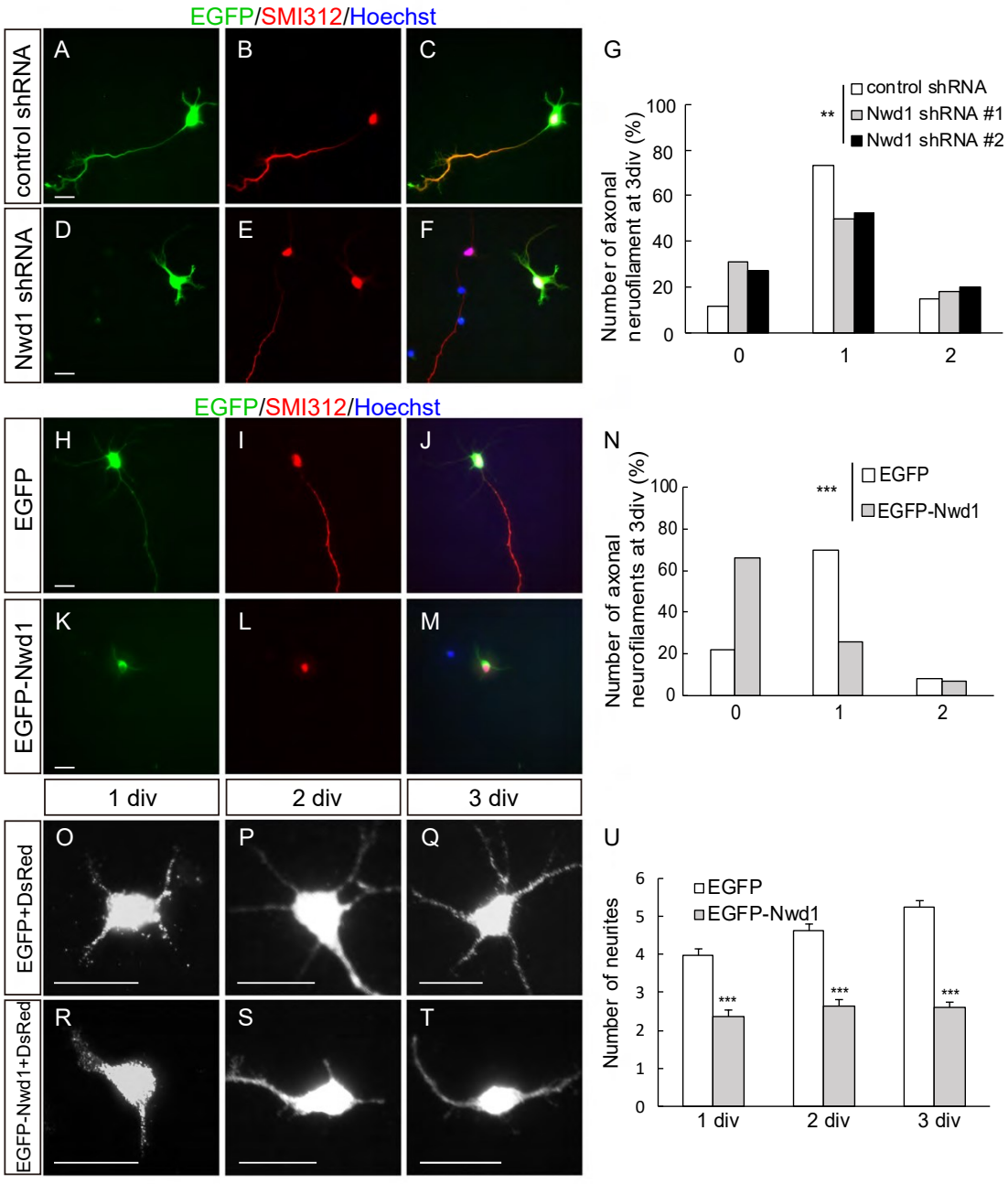
EGFP/SMI312/Hoechst
control shRNA
Nwd1 shRNA
A
B
C
D
E
F
G
control shRNA
Nwd1 shRNA #1
Nwd1 shRNA #2
**
Number of axonal neruofilament at 3div (%)
100
80
60
40
20
0
0
1
2
EGFP/SMI312/Hoechst
EGFP
EGFP-Nwd1
H
I
J
K
L
M
N
EGFP
EGFP-Nwd1
***
Number of axonal neurofilaments at 3div (%)
1 div
2 div
3 div
EGFP+DsRed
EGFP-Nwd1+DsRed
O
P
Q
R
S
T
U
EGFP
EGFP-Nwd1
Number of neurites
6
5
4
3
2
1
0
1 div
2 div
3 div

Figure 9. Tightly regulated Nwd1 expression is required for the induction of neuronal identity

(A–G) A non-targeting shRNA or *Nwd1* shRNAs were electroporated together with EGFP into primary cultured cortical neurons. Neurofilaments were stained with an anti-SMI312 antibody (red) at 3 div. (G) Number of $SMI312^+$ axons extending from a single neuron. $^{**}p<0.01$; control shRNA, n=101; shRNA #1, n=108; shRNA #2, n=99. (H–N) Cortical neurons transfected with EGFP-Nwd1 or control EGFP were stained for SMI312 at 3 div. (N) Number of $SMI312^+$ axons extending from a single neuron. $^{***}p<0.001$; EGFP, n=149; EGFP-Nwd1, n=149. (O–U) EGFP-Nwd1 or control EGFP were electroporated into cortical neurons and cultured for 1 div (O, R), 2 div (P, S), and 3 div (Q, T). To visualize fine immature neurites, a DsRed expression plasmid was co-electroporated into the cells. (U) Number of neurites extending from a single neuron. $^{***}p<0.01$; EGFP 1 div, n=150; 2 div, n=150; 3 div, n=200; EGFP-Nwd1 1 div, n=150; 2 div, n=150; 3 div, n=200. All data are presented as means ± SEM. Scale bars, 20 μm.

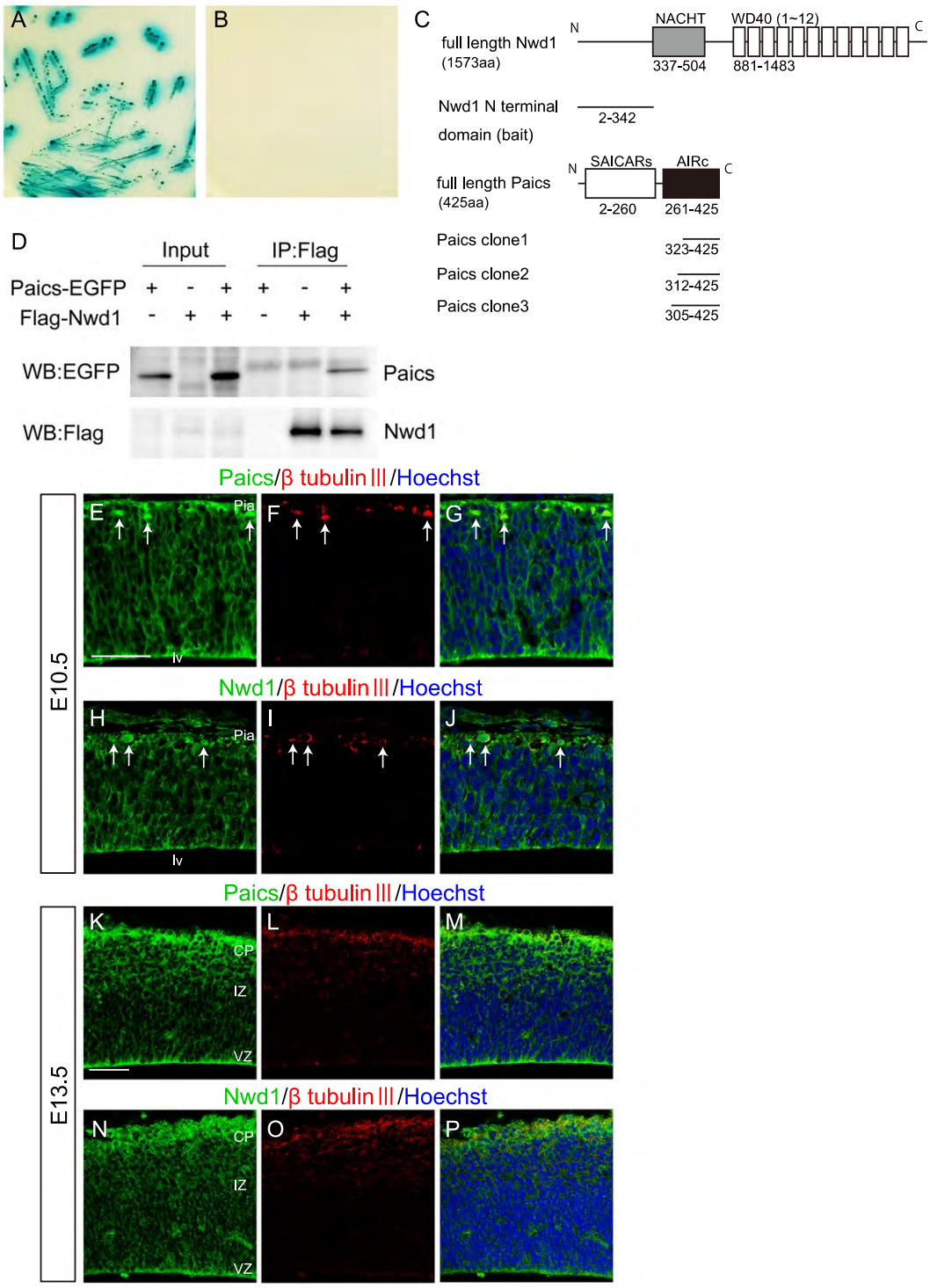
A
B
C
full length Nwd1
(1573aa)
N
NACHT
WD40 (1~12)
C
337-504
881-1483
Nwd1 N terminal
domain (bait)
2-342
full length Paics
(425aa)
N
SAICARs
AIRc
C
2-260
261-425
Paics clone1
323-425
Paics clone2
312-425
Paics clone3
305-425
D
Input
IP:Flag
Paics-EGFP + - + + - +
Flag-Nwd1 - + + - + +
WB:EGFP
Paics
WB:Flag
Nwd1
Paics/β tubulin III /Hoechst
E10.5
E
Pia
F
G
lv
Nwd1/β tubulin III /Hoechst
H
Pia
I
J
lv
Paics/β tubulin III /Hoechst
E13.5
K
CP
IZ
VZ
L
M
Nwd1/β tubulin III /Hoechst
N
CP
IZ
VZ
O
P

Figure 10. Nwd1 Interacts with Paics

(A and B) A yeast transformant with pGBKT7-Nwd1 (bait) and pGADT7-Paics (prey) was streaked on SD agar plates containing quadruple dropout media with Aureobasidin A and X-a-Gal, showing a positive interaction (A, blue colonies). The absence of colonies indicated the negative control (B). (C) Domain structure of the mouse Nwd1 and Paics proteins. The Nwd1 N-terminal region was used as a bait, and the isolated Paics cDNAs are indicated. Gray box, NACHT domain; open boxes, WD40 repeats; hatched box, SAICARs activity domain; black box, AIRc activity domain. (D) Co-IP showing the interaction between Nwd1 and Paics. HEK293 cells expressing FLAG-Nwd1 and/or Paics-EGFP were subjected to immunoprecipitation with an anti-FLAG antibody, followed by immunoblotting with anti-EGFP or anti-FLAG antibodies. (E–P) Telencephalon at E10.5 (E–J) and E13.5 (K–P) were double immunostained with anti-Paics (E, K) or anti-Nwd1 (H, N) and anti-b-tubulin III (F, I, L, O) antibodies. Arrows indicate b-tubulin III $^{+}$ neurons. Pia, Pial surface; lv, lateral ventricle. Scale bars, 50 μm in (E)–(P).

Table 1. Nwd1-binding partners identified by yeast two-hybrid screen

Each protein entry is shown with the respective NCBI accession number and the identified protein region. The respective protein functions are also listed.

Gene name	Gene Symbol	NCBI Reference Sequence: protein	Identified protein region (amino acids)	protein function
abhydrolase domain containing 3	Abhd3	NP_598891.1	350–411 aa	unknown, paralog of Abhd1
ATP-binding cassette, sub-family D (ALD), member 3	Abcd3	NP_033017.2	530–659 aa	peroxisomal import of fatty acids and/or fatty acyl-CoAs
chymotrypsin-like elastase family, member 1	Cela1	NP_291090.2	14–155 aa	protease associated with elastin remodeling
clavesin 2	Clvs2	NP_001346068.1	35–181 aa	recycling of synaptic vesicles
Kin17 DNA and RNA binding protein	Kin	NP_079556.1	1–188 aa	DNA/RNA binding protein
phosphoribosylaminoimidazole carboxylase, phosphoribosylaminoribosylaminoimidazole, succinocarboxamide synthetase	Paics	NP_080215.1	323–425 aa, 312–425 aa, 305–425 aa	*De novo* purine synthesis enzymes
quaking	Qk	NP_001152988.1	130–319 aa	RNA-binding protein
serine (or cysteine) peptidase inhibitor, clade E, member 2	Serpine2	NP_033281.1	307–397 aa	inhibititor for serine proteases
serine palmitoyltransferase, small subunit A	Sptssa	NP_598815.2	10–71 aa	serine palmitoyltransferase isoenzymes
E26 avian leukemia oncogene 1, 5' domain	Ets1	NP_001359463.1	1–111 aa	transcription factor
tripeptidyl peptidase II	Tpp2	NP_033444.1	1171–1261 aa	serine exopeptidase
WD repeat domain 74	Wdr74	NP_598900.1	114–378 aa	regulator of exosome complex formation

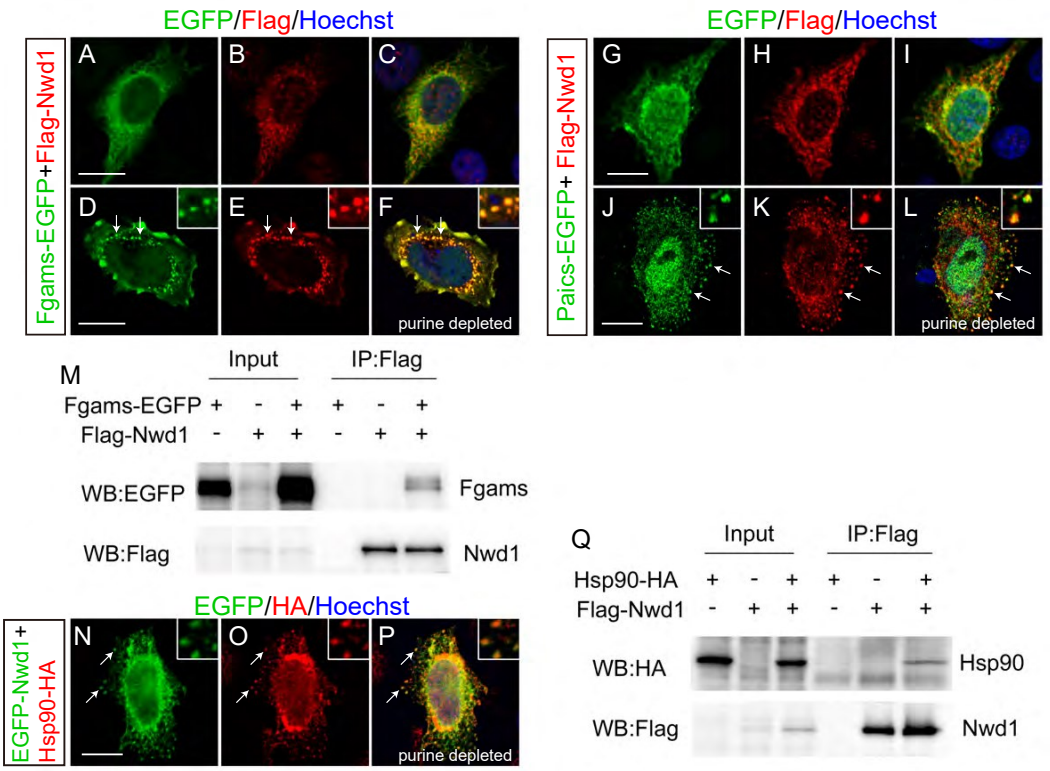

Figure 11. Nwd1 and Paics are localized in purinosomes

(A–L) HeLa cells were transfected with FLAG-Nwd1 (red) together with Fgams-EGFP (A–F) or Paics-EGFP (G–L) and cultured in complete medium (A–C and G–I) or in purine-depleted medium (D–F, J–L). Nwd1 was co-clustered with Fgams or Paics as purinosomes in purine-depleted medium (arrows). Nuclei were stained with Hoechst dye (blue). Insets in (D–F) and (J–L) showed the magnified view of the individual purinosomes formed in cytoplasm. (M) Co-IP showing the interaction between Nwd1 and Fgams. HEK293 cells expressing FLAG-Nwd1 and/or Fgams-EGFP were subjected to immunoprecipitation with an anti- FLAG antibody, followed by immunoblotting with anti-EGFP or anti-FLAG antibodies. (N–P) HeLa cells co-transfected with EGFP-Nwd1 (N) and Hsp90-HA (O) were cultured under purine-depleted conditions. (P) Merged

view. The arrows indicate the colocalization of Nwd1 and Hsp90 in purinosomes. Insets showed the high power photomicrograph of the individual purinosomes. (Q) Interaction between Nwd1 and Hsp90. HEK293 cells expressing Hsp90-HA and/or FLAG-Nwd1 were subjected to immunoprecipitation using an anti- FLAG antibody, followed by immunoblotting with an anti-HA or anti-FLAG antibody. Scale bars, 15μm.

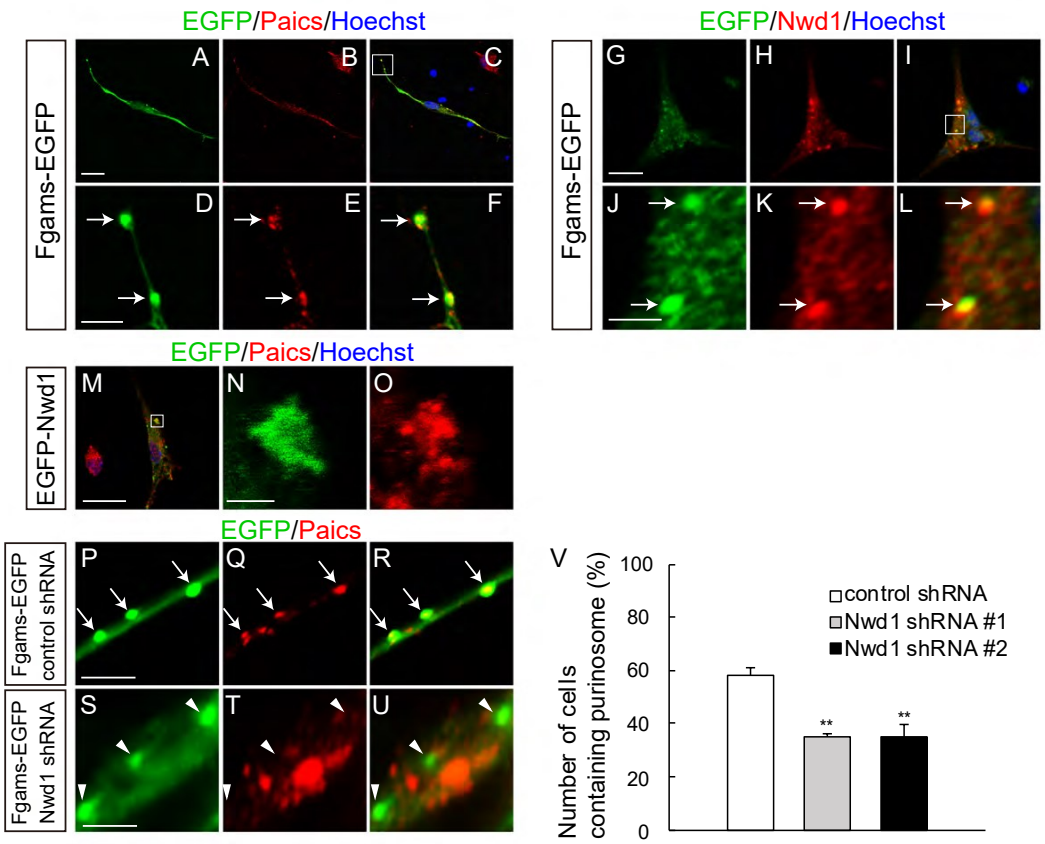

Figure 12. Nwd1 regulates purinosome assembly in NSPCs

(A–C) NSPCs derived from E12.5 telencephalons underwent electroporation with Fgams-EGFP (A) and were immunostained with an anti-Paics antibody (B, red) at 2 div. (C) Merged view. Nuclei (blue). (D–F) Higher magnification of the boxed area depicted in (C), showing the clustered signals of Fgams^{+} (D) Paics^{+} (E) purinosomes (arrows) in NSPCs. (F) Merged view. (G–L) Fgams-EGFP-expressing (G) NSPCs were immunostained with an anti-Nwd1 antibody (H). (I) Merged view. Nuclei (blue). (J–L) Higher magnification of the boxed area depicted in (I), demonstrating the localization of endogenous Nwd1 (K) in Fgams-EGFP^{+} (J) purinosomes. (L) Merged view.
(M) EGFP-Nwd1-expressing NSPCs were immunostained with an anti-Paics antibody. (N and O) Higher magnification of the boxed area depicted in (M), showing the

colocalization of EGFP-Nwd1 (N) and endogenous Paics (O) in purinosomes. (P–V) NSPCs were electroporated with the control shRNA (P–R) or Nwd1 shRNAs (S–U) together with Fgams-EGFP, followed by immunostaining with an anti-Paics antibody at 2 div. The arrows indicate the Fgams-EGFP^{+} Paics^{+} functional purinosomes in NSPCs. The arrowheads indicate the Fgams^{+} Paics^{-} cells. (V) Number of NSPCs containing Fgams-EGFP^{+} Paics^{+} purinosomes. Data are presented as means G SEM. **$p < 0.01$, Welch's t test followed by Holm-Bonferroni correction. Scale bars, 20 μm in (A)–(C) and (G)–(I), (M); 4 μm in (D)–(F), (J)–(L), and (P)–(U); 2 μm in (N), (O).

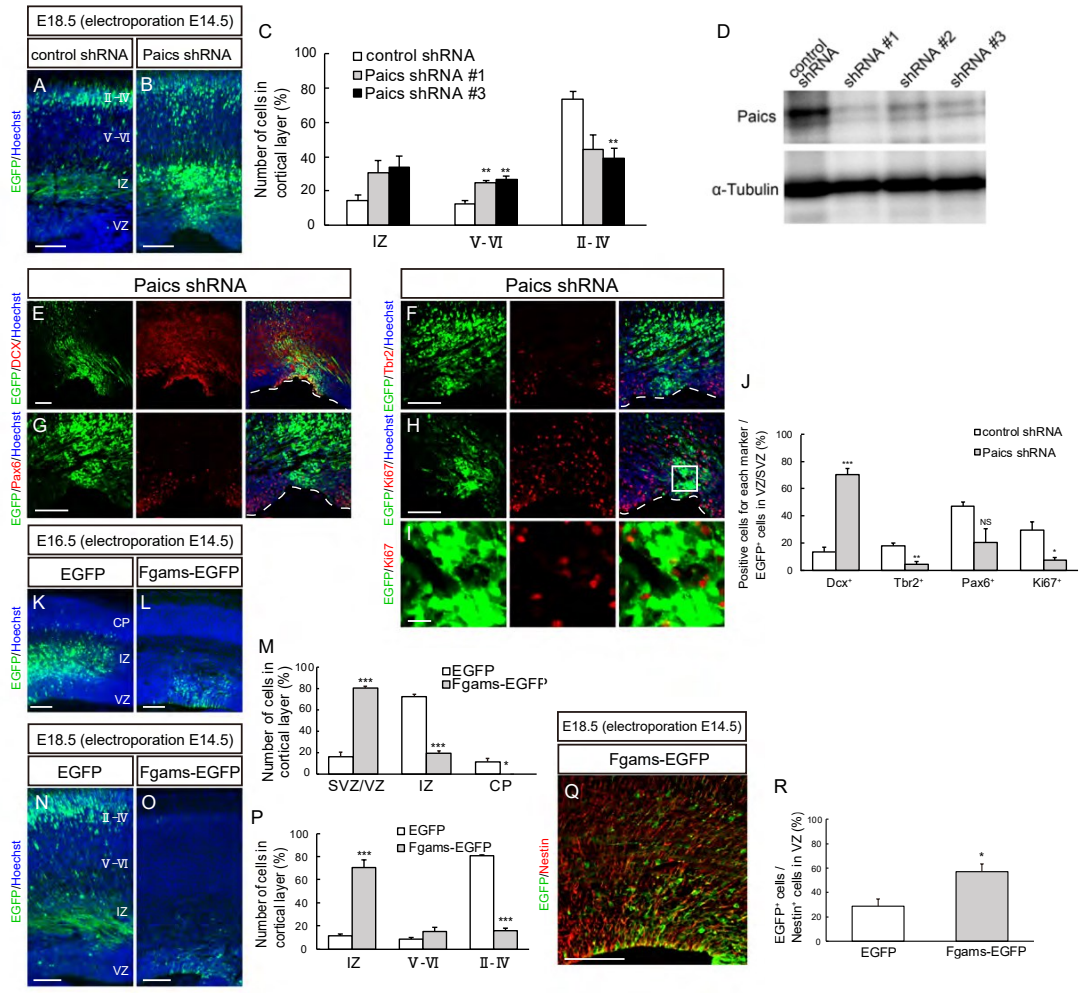

Figure 13. Purinosome components regulate cortical development

(A–J) A control shRNA or Paics shRNA (shRNA #1 or shRNA #3) was delivered into the brain on E14.5, together with EGFP, and the cortices were analyzed at E18.5. (A and B) Distribution of $EGFP^+$ cells in the neocortex. (C) Quantification of the distribution of $EGFP^+$ cells in the indicated areas. **$p < 0.01$. (D) N2a cells were transfected with three different mouse *Paics* shRNA constructs (shRNA #1, shRNA #2, and shRNA #3) or a non-targeting control shRNA, followed by immunoblotting with an anti-Paics or anti-α-tubulin antibody. (E–J) Brain sections of Paics knockdown were immunostained using anti-Dcx (E), anti-Pax6 (G), anti-Tbr2 (F), and anti-Ki67 (H and

I) antibodies. The VZ surface is outlined by the dashed line. (I) Higher magnification of the boxed area depicted in (H). (J) Graph shows the quantification of the positive cells for each marker to total $EGFP^+$ cells in the VZ/SVZ. NS, not significant, *p<0.05, **p<0.01, ***p<0.001. Note that the knockdown of Paics gene accelerates the mitotic exit of $Pac6^+$ or $Tbr2^+$ NSPCs and induces the premature expression of neuron marker Dcx. (K–R) Control EGFP or Fgams-EGFP was delivered into the brain on E14.5, and the cortices were analyzed at E16.5 (K and L) or E18.5 (N and O). (M and P) Distribution of $EGFP^+$ cells in the indicated areas at E16.5 (M) or E18.5 (P). *p < 0.05, ***p < 0.001. (Q) Fgams-EGFP-overexpressing brain immunostained with an anti Nestin antibody. (R) Quantification of Fgams-$EGFP^+$ cells to total $Nestin^+$ cells in VZ. *p<0.05. Forced expression of Fgams-EGFP directed many NSPCs to remain in the SVZ/VZ as $Nestin^+$ cells, and only a few cells reached the border between the SVZ and IZ. All data are presented as means G SEM. Statistical significance value was determined using the Welch's t test followed by Holm-Bonferroni correction. Scale bars, 100 μm in (A)–(H) and (K)–(Q); 15 μm in (I).

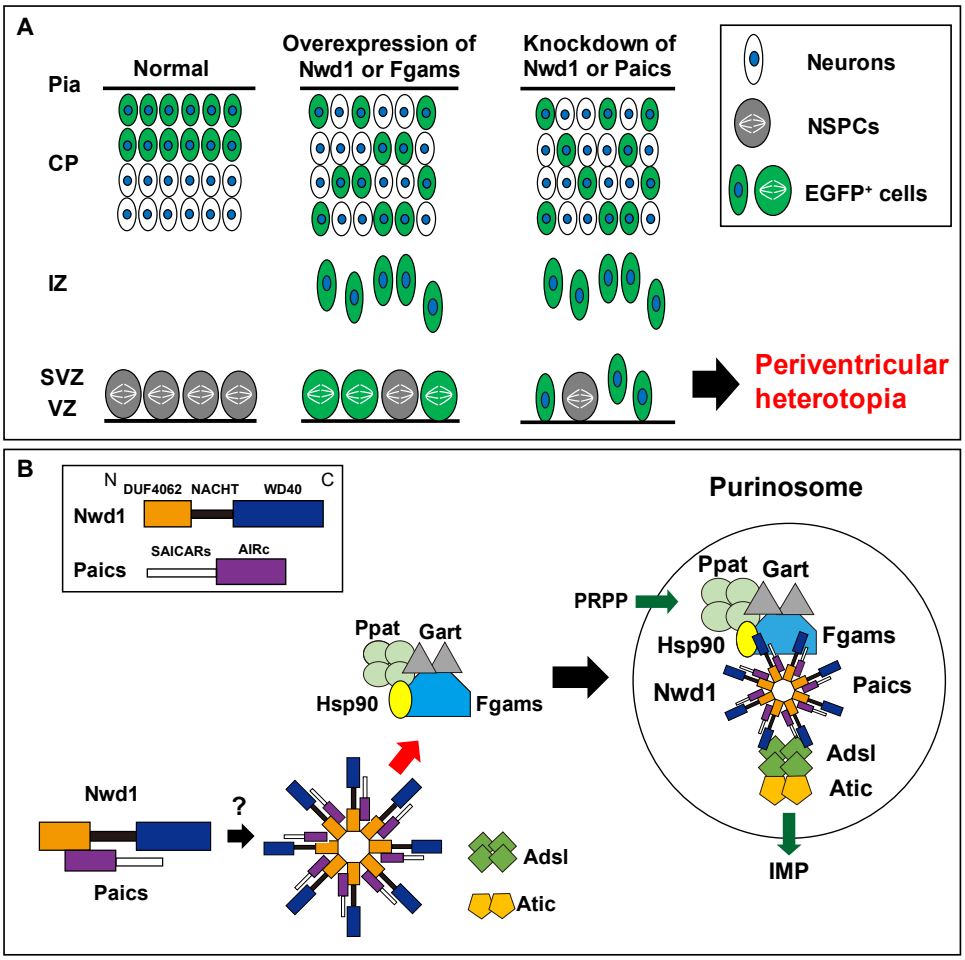

Figure 14. Models of Nwd1 Function in Corticogenesis and in Purinosome Formation

(A) Purinosome assembly/disassembly regulates cortical development. Overexpression of purinosome components (Nwd1 or Fgams) disturbs the radial migration of neurons and causes a significant increase in the Nestin^{+} NSPC pool in the VZ/SVZ. Knockdown of purinosome components (Nwd1 or Paics) accelerates mitotic exit and premature differentiation of NSPCs and represses neuronal migration leading to periventricular heterotopia. EGFP^{+} cells represent cells harboring the transgene.

(B) Hypothetical molecular model of purinosome formation by Nwd1. Undiscovered signals trigger the interaction of Nwd1 with Paics via the DUF4062 and AIRc domains, mediating the formation of the multimeric structure of Nwd1–Paics. The Nwd1–Paics complex systematically tethers other core enzymes, including Fgams, Ppat, and Gart, to form a functional purinosome. Nwd1, NACHT and WD repeat domain-containing protein 1; Ppat, phosphoribosyl pyrophosphate amidotransferase; Gart, phosphoribosylglycinamide formyltransferase; Fgams, formylglycin-amidine ribonucleotide synthase; Paics, phosphoribosylaminoimidazole carboxylase phosphoribosylaminoimidazole succinocarboxamide synthetase; Adsl, adenylosuccinate lyase; Atic, 5-aminoimidazole-4-carboxamide ribonucleotide formyltransferase inosine monophosphate cyclohydrolase; PRPP, phosphoribosyl diphosphate; IMP, inosine monophosphate; Hsp90, heat shock protein 90.

References

An, S., Deng, Y., Tomsho, J.W., Kyoung, M., and Benkovic, S.J. (2010). Microtubule-assisted mechanism for functional metabolic macromolecular complex formation. Proc. Natl. Acad. Sci. USA *107*, 12872–12876.

An, S., Kumar, R., Sheets, E.D., and Benkovic, S.J. (2008). Reversible compartmentalization of de novo purine biosynthetic complexes in living cells. Science *320*, 103–106.

Baresova, V., Skopova, V., Sikora, J., Patterson, D., Sovova, J., Zikanova, M., and Kmoch, S. (2012). Mutations of ATIC and ADSL affect purinosome assembly in cultured skin fibroblasts from patients with AICA-ribosiduria and ADSL deficiency. Hum. Mol. Genet. *21*, 1534–1543.

Baresova, V., Skopova, V., Souckova, O., Krijt, M., Kmoch, S., and Zikanova, M. (2018). Study of purinosome assembly in cell-based model systems with de novo purine synthesis and salvage pathway deficiencies. PLoS One 13, e0201432.

Barfeld, S.J., Fazli, L., Persson, M., Marjavaara, L., Urbanucci, A., Kaukoniemi, K.M., Rennie, P.S., Ceder, Y., Chabes, A., Visakorpi, T.*, et al.* (2015). Myc-dependent purine biosynthesis affects nucleolar stress and therapy response in prostate cancer. Oncotarget *6*, 12587–12602.

Battaglia, G., Chiapparini, L., Franceschetti, S., Freri, E., Tassi, L., Bassanini, S., Villani, F., Spreafico, R., D'Incerti, L., and Granata, T. (2006). Periventricular nodular heterotopia: classification, epileptic history, and genesis of epileptic discharges. Epilepsia 47, 86–97.

Cai, X., Xu, H., and Chen, Z.J. (2017). Prion-Like Polymerization in Immunity and Inflammation. Cold Spring Harb. Perspect. Biol. *9*, a023580.

Chakravarthi, B., Goswami, M.T., Pathi, S.S., Dodson, M., Chandrashekar, D.S., Agarwal, S., Nepal, S., Hodigere Balasubramanya, S.A., Siddiqui, J., Lonigro, R.J.*, et*

al. (2018). Expression and role of PAICS, a de novo purine biosynthetic gene in prostate cancer. Prostate *78*, 693–694.

Chan, C.Y., Zhao, H., Pugh, R.J., Pedley, A.M., French, J., Jones, S.A., Zhuang, X., Jinnah, H., Huang, T.J., and Benkovic, S.J. (2015). Purinosome formation as a function of the cell cycle. Proc. Natl. Acad. Sci. USA *112*, 1368–1373.

Correa, R.G., Krajewska, M., Ware, C.F., Gerlic, M., and Reed, J.C. (2014). The NLR-related protein NWD1 is associated with prostate cancer and modulates androgen receptor signaling. Oncotarget *5*, 1666–1682.

Cossu, M., Mirandola, L., and Tassi, L. (2018). RF-ablation in periventricular heterotopia-related epilepsy. Epilepsy Res. *142*, 121–125.

Dorstyn, L., Akey, C.W., and Kumar, S. (2018). New insights into apoptosome structure and function. Cell. Death. Differ. *25*, 1194–1208.

Englund, C., Fink, A., Lau, C., Pham, D., Daza, R.A., Bulfone, A., Kowalczyk, T., and Hevner, R.F. (2005). Pax6, Tbr2, and Tbr1 are expressed sequentially by radial glia, intermediate progenitor cells, and postmitotic neurons in developing neocortex. J. Neurosci. *25*, 247–251.

Finn, R.D., Attwood, T.K., Babbitt, P.C., Bateman, A., Bork, P., Bridge, A.J., Chang, H.-Y., Dosztányi, Z., El-Gebali, S., and Fraser, M. (2017). InterPro in 2017—beyond protein family and domain annotations. Nucl. acid. res. *45*, D190–D199.

French, J.B., Zhao, H., An, S., Niessen, S., Deng, Y., Cravatt, B.F., and Benkovic, S.J. (2013). Hsp70/Hsp90 chaperone machinery is involved in the assembly of the purinosome. Proc. Natl. Acad. Sci. USA *110*, 2528–2533.

French, J.B., Jones, S.A., Deng, H., Pedley, A.M., Kim, D., Chan, C.Y., Hu, H., Pugh, R.J., Zhao, H., Zhang, Y.*, et al.* (2016). Spatial colocalization and functional link of purinosomes with mitochondria. Science *351*, 733–737.

Garcia-Cardena, G., Fan, R., Shah, V., Sorrentino, R., Cirino, G., Papapetropoulos, A., and Sessa, W.C. (1998). Dynamic activation of endothelial nitric oxide synthase by Hsp90. Nature *392*, 821–824.

Gottle, M., Burhenne, H., Sutcliffe, D., and Jinnah, H.A. (2013). Purine metabolism during neuronal differentiation: the relevance of purine synthesis and recycling. J. Neurochem. *127*, 805–818.

Hansen, A.H., Duellberg, C., Mieck, C., Loose, M., and Hippenmeyer, S. (2017). Cell Polarity in Cerebral Cortex Development-Cellular Architecture Shaped by Biochemical Networks. Front. Cell. Neurosci. *11*.176

Hirota, Y., and Nakajima, K. (2017). Control of Neuronal Migration and Aggregation by Reelin Signaling in the Developing Cerebr Cortex. Front. Cell. Dev. Biol. *5*, 40.

Iwasaki, Y., Yumoto, T., and Sakakibara, S. (2015). Expression profiles of inka2 in the murine nervous system. Gene. Expr. Patterns. *19*, 83–97.

Jurecka, A., Zikanova, M., Kmoch, S., and Tylki-Szymanska, A. (2015). Adenylosuccinate lyase deficiency. J. Inherit. Metab. Dis. *38*, 231–242.

Kawai, S., Takagi, Y., Kaneko, S., and Kurosawa, T. (2011). Effect of Three Types of Mixed Anesthetic Agents Alternate to Ketamine in Mice. Exp. Anim. *60*, 481–487.

Konno, D., Yoshimura, S., Hori, K., Maruoka, H., and Sobue, K. (2005). Involvement of the phosphatidylinositol 3-kinase/rac1 and cdc42 pathways in radial migration of cortical neurons. J. Biol. Chem. *280*, 5082–5088.

Leipe, D.D., Koonin, E.V., and Aravind, L. (2004). STAND, a class of P-loop NTPases including animal and plant regulators of programmed cell death: multiple, complex domain architectures, unusual phyletic patterns, and evolution by horizontal gene transfer. J. Mol. Biol. *343*, 1–28.

Li, P., Nijhawan, D., Budihardjo, I., Srinivasula, S.M., Ahmad, M., Alnemri, E.S., and Wang, X. (1997). Cytochrome c and dATP-dependent formation of Apaf-1/caspase-9 complex initiates an apoptotic protease cascade. Cell *91*, 479–489.

Li, S.X., Tong, Y.P., Xie, X.C., Wang, Q.H., Zhou, H.N., Han, Y., Zhang, Z.Y., Gao, W., Li, S.G., Zhang, X.C.*, et al.* (2007). Octameric structure of the human bifunctional enzyme PAICS in purine biosynthesis. J. Mol. Biol. *366*, 1603–1614.

Li, Y., Wang, J., Zhou, Y., Li, D., and Xiong, Z.Q. (2015). Rcan1 deficiency impairs neuronal migration and causes periventricular heterotopia. J. Neurosci. *35*, 610–620.

Lian, G., and Sheen, V.L. (2015). Cytoskeletal proteins in cortical development and disease: actin associated proteins in periventricular heterotopia. Front. Cell. Neurosci. *9*, 99.

Lin, J.H., Takano, T., Arcuino, G., Wang, X., Hu, F., Darzynkiewicz, Z., Nunes, M., Goldman, S.A., and Nedergaard, M. (2007). Purinergic signaling regulates neural progenitor cell expansion and neurogenesis. Dev. Biol. *302*, 356–366.

Liu, X., Hashimoto-Torii, K., Torii, M., Haydar, T.F., and Rakic, P. (2008). The role of ATP signaling in the migration of intermediate neuronal progenitors to the neocortical subventricular zone. Proc. Natl. Acad. Sci. USA *105*, 11802–11807.

Makhnevych, T., and Houry, W.A. (2012). The role of Hsp90 in protein complex assembly. Biochim. Biophys. Acta. *1823*, 674–682.

Marie, S., Heron, B., Bitoun, P., Timmerman, T., Van Den Berghe, G., and Vincent, M.F. (2004). AICA-ribosiduria: a novel, neurologically devastating inborn error of purine biosynthesis caused by mutation of ATIC. Am. J. Hum. Genet. *74*, 1276–1281.

Matsuda, T., and Cepko, C.L. (2004). Electroporation and RNA interference in the rodent retina in vivo and in vitro. Proc. Natl. Acad. Sci. USA *101*, 16–22.

Meng, M., Chen, Y., Jia, J., Li, L., and Yang, S. (2018). Knockdown of PAICS inhibits malignant proliferation of human breast cancer cell lines. Biol. Res. *51*.24

Mermigka, G., Amprazi, M., Mentzelopoulou, A., Amartolou, A., and Sarris, P.F. (2020). Plant and Animal Innate Immunity Complexes: Fighting Different Enemies with Similar Weapons. Trends. Plant. Sci. *25*, 80–91.

Miller, J.A., Nathanson, J., Franjic, D., Shim, S., Dalley, R.A., Shapouri, S., Smith, K.A., Sunkin, S.M., Bernard, A., and Bennett, J.L. (2013). Conserved molecular signatures of neurogenesis in the hippocampal subgranular zone of rodents and primates. Development. *140*, 4633–4644.

Ohtaka-Maruyama, C., and Okado, H. (2015). Molecular Pathways Underlying Projection Neuron Production and Migration during Cerebral Cortical Development. Front. Neurosci. *9*, 447.

Pedley, A.M., and Benkovic, S.J. (2017). A New View into the Regulation of Purine Metabolism: The Purinosome. Trends. Biochem. Sci. *42*, 141–154.

Pelet, A., Skopova, V., Steuerwald, U., Baresova, V., Zarhrate, M., Plaza, J.M., Hnizda, A., Krijt, M., Souckova, O., Wibrand, F.*, et al.* (2019). PAICS deficiency, a new defect of de novo purine synthesis resulting in multiple congenital anomalies and fatal outcome. Hum. Mol. Genet. *28*, 3805–3814.

Pelham, H.R. (1990). The retention signal for soluble proteins of the endoplasmic reticulum. Trends. Biochem. Sci. *15*, 483-486.

Raman, R., Pinto, C.S., and Sonawane, M. (2018). Polarized Organization of the Cytoskeleton: Regulation by Cell Polarity Proteins. J. Mol. Biol. *430*, 3565–3584.

Represa, A. (2019). Why Malformations of Cortical Development Cause Epilepsy. Front. Neurosci. *13*. 250

Riedl, S.J., and Salvesen, G.S. (2007). The apoptosome: signalling platform of cell death. Nat. Rev. Mole. Cell. Biol. *8*, 405–413.

Sakakibara, S., and Okano, H. (1997). Expression of neural RNA-binding proteins in the postnatal CNS: implications of their roles in neuronal and glial cell development. J. Neurosci. *17*, 8300–8312.

Sakakibara, S., Nakamura, Y., Satoh, H., and Okano, H. (2001). RNA-Binding Protein Musashi2: Developmentally Regulated Expression in Neural Precursor Cells and Subpopulations of Neurons in Mammalian CNS. J. Neurosci. *21*, 8091–8107.

Scott, C.E., Wynn, S.L., Sesay, A., Cruz, C., Cheung, M., Gaviro, M.V.G., Booth, S., Gao, B., Cheah, K.S.E., Lovell-Badge, R.*, et al.* (2010). SOX9, acting downstream of Sonic hedgehog signalling, induces and maintains neural stem cells. Nat. Neurosci. *13*, 1181–1189.

Sessa, A., Mao, C.A., Hadjantonakis, A.K., Klein, W.H., and Broccoli, V. (2008). Tbr2 directs conversion of radial glia into basal precursors and guides neuronal amplification by indirect neurogenesis in the developing neocortex. Neuron *60*, 56–69.

Traut, T.W. (1994). Physiological concentrations of purines and pyrimidines. Mol. Cell. Biochem. *140*, 1–22.

Yamaoka, T., Kondo, M., Honda, S., Iwahana, H., Moritani, M., Ii, S., Yoshimoto, L., and Itakura, M. (1997). Amidophosphoribosyltransferase Limits the Rate of Cell Growth-linked de Novo Purine Biosynthesis in the Presence of Constant Capacity of Salvage Purine Biosynthesis. J. Biol. Chem. *272*, 17719–17725.

Yang, Q., Huang, Z., Luo, Y., Zheng, F., Hu, Y., Liu, H., Zhu, S., He, M., Xu, D., Li, Y.*, et al.* (2019). Inhibition of Nwd1 activity attenuates neuronal hyperexcitability and GluN2B phosphorylation in the hippocampus. EBioMed. *47*, 470–483.

Yumoto, T., Nakadate, K., Nakamura, Y., Sugitani, Y., Sugitani-Yoshida, R., Ueda, S., and Sakakibara, S. (2013). Radmis, a novel mitotic spindle protein that functions in cell division of neural progenitors. PLoS One *8*, e79895.

Zhao, C., Deng, W., and Gage, F.H. (2008). Mechanisms and functional implications of adult neurogenesis. Cell *132*, 645–660.

Zou, H., Li, Y., Liu, X., and Wang, X. (1999). An APAF-1·Cytochrome c Multimeric Complex Is a Functional Apoptosome That Activates Procaspase-9. J. Biol. Chem. *274*, 11549–11556.

Acknowledgements

I would like to express my deepest gratitude to Dr. Shin-ichi Sakakibara for study concept and design, technical assistance, and drafting of the manuscript. I would also like to express my gratitude to Dr. Masaki Kakeyama and Dr. Taichi Hara for vice chair in my doctoral dissertation. I would also like to thank Dr. Hiroki Akiyama and the members of the Sakakibara Laboratory for their advice. I would like to express my gratitude to them.